

COMPARISON BETWEEN THE DYNAMIC RESPONSE OF SELECTIVE LASER
MELTING (SLM) PARTS AND CONVENTIONALLY MANUFACTURED PARTS

A thesis presented to the faculty of the Graduate School of
Western Carolina University in partial fulfillment of the
requirements for the degree of Master of Science in Technology

By:
Lee Clark Sechrest

Advisor: Dr. Sudhir Kaul
School of Engineering & Technology

Committee Members:
Dr. Patrick Gardner, School of Engineering and Technology
Dr. Wesley Stone, School of Engineering and Technology

November 2016

TABLE OF CONTENTS

List of Tables	iii
List of Figures	iv
Abstract	v
Chapter 1: Introduction	1
1.1 Scope of Thesis	2
1.2 Overview of Thesis	3
1.3 Key Terms	3
Chapter 2: Literature Review	5
2.1 Overview	5
2.2 Testing Method	6
2.2.1 Static Testing	6
2.2.2 Dynamic Testing	6
2.2.2.1 Laser Vibrometry	7
2.3 History & Current Technology	7
2.3.1 History	7
2.3.2 Current Technology	11
2.4 Summary	12
Chapter 3: Mathematical Modeling	13
3.1 Beam Modeling	13
3.2 Results	18
3.2.1 Frequency Response	18
3.2.2 Natural Frequencies and Mode Shapes	19
3.3 Summary	21
Chapter 4: Experimental Results	22
4.1 Test Equipment	22
4.2 Experimental Setup – Static Testing	24
4.3 Experimental Setup – Dynamic Testing	25
4.4 Results – Static Testing	28
4.5 Results – Dynamic Testing	31
4.6 Summary	36
Chapter 5: Conclusions and Future Research	37
5.1 Conclusions	37
5.2 Future Scope	39
References	42
Appendix A	44
Appendix B	51

LIST OF TABLES

Table 3.1: Calculated Natural Frequencies	22
Table 4.1: Tensile Test Results	29
Table 4.2: Comparison - Averages	29
Table 4.3: Results – T-Test – Ultimate Tensile Stress.....	30
Table 4.4: Results – T-Test – Elastic Modulus.....	30
Table 4.5: Build Parameter Legend	32
Table 4.6: Natural Frequency Results.....	32
Table 4.7: Damping Results.....	35

LIST OF FIGURES

Figure 3.1: Static Deflection Model.....	14
Figure 3.2: Bending Deflection – Static Load	15
Figure 3.3: Mode Shape Model	17
Figure 3.4: Equivalent Frequency Response	17
Figure 3.5: Calculation of Frequency Response	18
Figure 3.6: Frequency Response – Cantilever Beam.....	19
Figure 3.7: First Mode Shape (Bending)	20
Figure 3.8: Second Mode Shape (Bending).....	20
Figure 3.9: Third Mode Shape (Bending).....	20
Figure 4.1: EOS M290 SLM 3D Printer.....	22
Figure 4.2: Instron 5967 Tensile Tester.....	23
Figure 4.3: Polytech PSV-400 Scanning Laser Vibrometer	24
Figure 4.4: Vibrometer Test Layout	26
Figure 4.5: Picture of Test Setup	27
Figure 4.6: Scan Grid of the Beam	27
Figure 4.7: Frequency Response.....	33
Figure 4.8: Frequency Response – Around Second Frequency	33
Figure 4.9: Frequency Response – Around Third Frequency.....	34

ABSTRACT

COMPARISON BETWEEN THE DYNAMIC RESPONSE OF SELECTIVE LASER MELTING (SLM) PARTS AND CONVENTIONALLY MANUFACTURED PARTS

Lee Clark Sechrest, M.S.T.

Western Carolina University (November 2016)

Advisor: Dr. Sudhir Kaul

Selective Laser Melting (SLM) is a relatively new manufacturing process in additive manufacturing (commonly referred to as 3D printing). The process uses a laser sintering technique to build metal parts layer by layer by using the raw material in a powder form. A high intensity laser is used to melt each layer of the metal powder and attach it to the rest of the part. This process is a significant enhancement of additive manufacturing processes since it can be used to manufacture production parts, not just rapid prototypes for visual or educational use. The goal of this research has been to determine the main distinctions between parts made by SLM and parts made by conventional manufacturing processes such as rolling or forging. Specifically, dynamic response and dynamic properties have been compared in this research. Properties such as tensile strength, hardness, natural modes etc. have also been investigated. The dynamic properties have been compared by using simple geometries such as beam structures and relatively complex geometries such as small turbine wheels. A laser vibrometer and a tensile tester have been used to perform all the testing for dynamic and static characterization. Test results have provided a comprehensive understanding of the structural properties of parts made by the SLM process. Test results have also provided some insight into the influence of process parameters on the dynamic properties of the parts manufactured by SLM. The overarching aim of this research has been to determine whether parts manufactured by this new additive

manufacturing technique are comparable to conventionally manufactured parts. Results indicate that the static properties (tensile strength, yield strength, etc.) of parts manufactured by SLM are statistically similar to other parts. Also, static properties are not seen to vary significantly with the choice of parameters associated with the SLM process. However, it is observed that the damping ratios corresponding to the bending modes are higher for parts made by SLM, regardless of process parameters. It is also observed that natural frequencies corresponding to the bending modes decrease while natural frequencies corresponding to the torsional modes increase. Furthermore, parameters such as layer thickness and number of scans are seen to significantly influence the natural frequency. These observations indicate that the fatigue life of parts made by SLM can vary significantly. Therefore, the choice of process parameters needs to be investigated further, and it may be necessary to make modifications to the geometry of a part

CHAPTER 1: INTRODUCTION

Material properties play a significant role in all commercial applications. The dynamic response of materials is particularly important for components that are expected to withstand dynamic loads during the life of a product. Selective laser melting (SLM) is a process in additive manufacturing (commonly referred to as 3D printing) that uses the raw material in a powder form and develops the geometry of a part from the three dimensional (3D) model. The geometry is developed layer-by-layer and a high intensity laser is used to melt each layer of the metal powder and attach it to the rest of the part. This manufacturing process has generated a significant amount of interest since it can be used to manufacture production parts. Although there are multiple 3D printing processes such as fused deposition modeling (FDM), stereolithography, etc. that have been prevalent for the last two decades, these processes have been mostly limited to the development of non-functional prototypes. This has made the emergence of SLM a significant development in additive manufacturing since this process can be used to make functional parts with a material that may be used for production, significantly cutting down the development time. Multiple researchers have been investigating the pros and cons of the SLM process and some common issues that have been identified include porosity, surface finish, and post-processing to remove support material. Some of the research has focused on using re-melting as a possible means of reducing porosity and enhancing the density of the parts manufactured by SLM to improve fatigue life characteristics.

This study investigates the dynamic properties of parts made from the SLM process and compares these properties with similar parts that are made from alternative manufacturing

processes such as rolling, forging or machining. Some of the process parameters that may play a significant role are also investigated. This thesis seeks to answer the following questions:

1. Are the dynamic properties of parts manufactured by the SLM process different from other manufacturing processes? If so, how?
2. Do the process parameters play a significant role in determining the dynamic response of parts made by the SLM process?
3. What are the implications of the differences in the dynamic response, if any?

1.1 Scope of Thesis

This thesis investigates the build parameters of SLM and their influence on the dynamic response of the material. This is important because as the technology grows, the capabilities of this process are expected to evolve. SLM is expected to become a viable manufacturing process in the long term. This research investigates the dynamic and static properties of parts manufactured through the SLM process and directly compares the properties with parts made through traditional processes. A mathematical model is developed to establish a baseline and reference for the experimental investigation.

Multiple iterations of experimental investigation have been carried out. This included testing static properties such as tensile strength, yield strength, and hardness. These tests were followed by testing cantilever beams with the use of a laser vibrometer. The frequency response of the tested beams was used to determine the damping ratio, the natural frequency and the natural mode of these parts. These results were compared for the standard setting of the SLM machine. Further testing was performed by changing the process parameters. Only two process parameters were investigated – number of scans and layer thickness.

1.2 Overview of Thesis

This thesis presents a brief history of the evolution of additive manufacturing and metal 3D printing. Some of the advantages and challenges associated with the SLM are discussed along with a review of the current literature in Chapter 2.

Chapter 3 presents the mathematical model of the system and the expected results from dynamic testing. This model is useful for establishing a reference and a baseline. Chapter 4 presents the experimental setup and the results. The results are analyzed and discussed in Chapter 4. Chapter 5 summarizes the main findings of this study and provides a scope of future research that can be carried out in the near future.

1.3 Key Terms

3D scanning, noun — a method of acquiring the shape and size of an object as a 3-dimensional representation by recording x,y,z coordinates on the object's surface and through software by collecting points that are converted into digital data (ASTM, 2015).

Additive Manufacturing (AM), noun —a process of joining material to make objects from 3D models, usually layer upon layer, as opposed to subtractive manufacturing methodologies.

Build platform, noun — of a machine, any base which provides a surface upon which the build is started and supported throughout the build process (ASTM, 2015).

Build surface, noun — area where material is added, normally on the last deposited layer which becomes the foundation upon which the next layer is formed (ASTM, 2015).

CNC, noun — Computer Numerical Control, computerized control of machines for manufacturing (ASTM, 2015).

Direct metal laser sintering (DMLS[®]), noun — a powder bed fusion process used to make metal parts directly from metal powders without intermediate “green” or “brown” parts; term denotes

metal-based laser sintering systems from EOS GmbH – Electro Optical Systems. Synonym: direct metal laser melting (ASTM, 2015).

Fused deposition modeling (FDM[®]), noun — a material extrusion process used to make thermoplastic parts through heated extrusion and deposition of materials layer by layer; term denotes machines built by Stratasys, Inc (ASTM, 2015).

Laser Sintering (LS), noun — a powder bed fusion process used to produce objects from powdered materials using one or more lasers to selectively fuse or melt the particles at the surface, layer by layer, in an enclosed chamber (ASTM, 2015).

Reverse engineering, noun — in additive manufacturing, a method of creating a digital representation from a physical object to define its shape, dimensions, and internal and external features (ASTM, 2015).

Selective laser Sintering (SLS) — denotes the LS process and machines from 3D Systems Corporation (ASTM, 2015).

Stereolithography (SL), noun — a photopolymerization process used to produce parts from photopolymer materials in a liquid state using one or more lasers to selectively cure to a predetermined thickness and harden the material into shape, layer upon layer (ASTM, 2015).

STL, noun — in additive manufacturing, file format for 3D model data used by machines to build physical parts; STL is the de facto standard interface for additive manufacturing systems. STL originated from the term stereolithography (ASTM, 2015).

Subtractive manufacturing, noun — making objects by the removal of material (for example, milling, drilling, grinding, carving, etc.) from a bulk solid to leave a desired shape, as opposed to additive manufacturing (ASTM, 2015).

CHAPTER 2: LITERATURE REVIEW

This chapter provides the background for this study along with a review of the literature that has been used for reference during different stages of the research. The properties of parts manufactured through additive manufacturing are discussed in addition to some of the recent findings reported in the literature.

2.1 Overview

Selective laser melting (SLM) is an additive manufacturing method that is also referred to as 3D printing. SLM is one of the largest growing segments of the 3D printing industry. While additive manufacturing was being primarily used in prototyping in the past, the speed and accuracy of manufacturing parts in metal is making the process viable for production purposes or for making a large number of parts that may not be limited to prototypes. When metal 3D printing was in its infancy, parts were manufactured by using selective laser sintering (SLS). SLS 3D printing is a process where the individual metal powder particles are heated and then fused together with the surrounding metal particles, layer by layer. The SLS process produces parts with a much lower ultimate strength than the parts manufactured through other processes. This is largely due to stresses produced within the part, these stresses lower the ultimate strength of the part closer to the normal yield strength of the material, as reported in the literature (Vrancken, 2014). During the selective laser melting process, a larger melt pool is created, this melt pool penetrates multiple layers of the part that are created. By penetrating multiple layers with the melt pool, the part being created has a much higher strength than those produced by the laser sintering process. As the accuracy of these parts is improving with the advancement of the SLM machines, it is becoming possible to substitute these parts for those produced with traditional

methods. However, currently there is limited knowledge about the dynamic properties of parts produced through the SLM process. This study aims to investigate the dynamic properties in addition to specific static properties of parts made through the SLM process and compare the properties with similar parts made through conventional manufacturing processes.

2.2 Testing Method

This section provides a brief description of the methods used for testing the static and dynamic properties of parts made by using the SLM process.

2.2.1 Static Testing

Tensile testing can be used to determine the stress-strain characteristics and properties such as yield strength, ultimate tensile strength and modulus of elasticity of the material. By mechanically increasing the strain on the work piece and measuring the corresponding load, the load-deflection and the stress-strain diagrams can be plotted to determine the characteristics used to identify strength as well as stiffness of the material. The test is typically performed at very low strain rates. Some of the static material properties are also important in determining the dynamic behavior of material. In addition to tensile testing, hardness testing was performed in this study to compare the ability of the surface to withstand indentation.

2.2.2 Dynamic Testing

Dynamics testing is used to determine the properties of a material that may be subject to loads at higher strain rates. Materials are known to exhibit significantly different behavior at relatively higher strain rates that may include hysteresis, strain hardening, etc. The dynamic properties, are therefore, important for parts that may need to work in an environment with time varying loads. If the dynamic properties of a material are not well understood, then a part could

be exposed to stresses that reduce the life of the product significantly even if the static strength of the material is relatively high. Dynamic properties can be measured through multiple means to quantify the fatigue life. In this study, laser vibrometry and ping testing have been primarily used to evaluate the dynamic properties of parts by the SLM process.

2.2.2.1 Laser Vibrometry

A 3-D scanning laser vibrometer is used to measure the vibrations within a given part that is subject to external excitation. The scanner compares the light emitted from the vibrometer to the light returning from the surface of the part. The light that bounces off the vibrating surface is shifted in frequency and phase, this is called as the Doppler Effect. This light is compared to the original light produced by the laser, the changes in frequency and phase of the light can be used to determine the vibrations of the surface including the resonant frequencies. This is a non-contact method that is preferable to the use of an accelerometer since there are no sensors that need to be attached to the part. The excitation input can be directly mounted on the test part, if needed.

2.3 History & Current Technology

A brief description of the recent history of additive manufacturing is provided in this section. The current state of the 3D metal printing processes is also discussed in this section.

2.3.1 History

Selective laser melting (SLM) is a process in additive manufacturing (commonly referred to as 3D printing) that uses the raw material in a powder form and develops the geometry of a part from the three dimensional (3D) model. The geometry is developed layer-by-layer and a high intensity laser is used to melt each layer of the metal powder and attach it to the rest of the part. This manufacturing process has generated a significant amount of interest since it can be

used to manufacture production parts or functional prototypes, and not just rapid prototypes for visual or educational purposes. Although there are multiple 3D printing processes such as fused deposition modeling (FDM), stereolithography, etc. that have been prevalent for the last two decades, these processes have been mostly limited to the development of non-functional prototypes. This has made the emergence of SLM a significant development in additive manufacturing since this process can be used to make functional parts with a material that may be used for production. Multiple researchers have been investigating the pros and cons of the SLM process and some common issues that have been identified include porosity, surface finish and post-processing to remove support material. Some of the research has focused on using re-melting as a possible means of reducing porosity and enhancing the density of the parts manufacture by SLM to improve fatigue life characteristics.

EOS began their work into the research of using SLM for manufacturing 3D printed parts in 1989. However, the basis of this technology began with the research of Dr. Carl Deckard at the University of Texas at Austin in the mid 1980's (http://www.me.utexas.edu/news/2012/0712_sls_history.php). During his senior year at the university, Dr. Deckard had the idea of using an energy beam to melt particles of powder together to make a part. After designing the basis of a selective laser sintering (SLS) system during his graduate studies, Dr. Deckard paired with Dr. McClure and Harold Blair to commercialize the technology (Lou, 2012). The company they formed to produce this technology was called Nova Automation. With this new company, Dr. Deckard began to produce better machines and ultimately machines with industrial capabilities. In 1993, Dr. Deckard left the company to become a professor at Clemson University. After leaving Clemson and returning to Texas, Dr. Deckard began research in materials science and producing additional materials for

additive manufacturing. Ultimately his company DTP was sold to 3D Systems, one of the largest producers of 3D printing technologies today (Lou, 2012). Using the technology created by Dr. Deckard, 3D Systems has become one of the industry giants, and they currently produce both plastic and metal SLS 3D printers for the industrial markets. However, 3D Systems is still working with SLS technology that was originally designed by Dr. Deckard. As the additive manufacturing market has evolved, companies like EOS have moved from SLS into SLM printing because of specific advantages with the strength of the end product. Due to the versatility of the SLM process, the machines that are currently available are making it possible to move from “rapid prototyping” technologies to “rapid production” technologies with a significantly lower turnaround time from design conception to production. For this to become a reality in the near future, multiple advances need to happen in the near future that will modify the machines that are currently in use. The machines would need to become less expensive and the maintenance and operation of these machines needs to become less complex and cumbersome (David, 2014). As SLM 3D printers move into the production market, there can be a number of economic benefits. For instance, these machines allow for the recycling of material not used in each production run, meaning that there is little to no waste in the production of each part. If the production time for the machines is decreased over time, it could eliminate the need for companies to inventory various sizes of material in stock because all parts are produced from one stock, the same powder (David, 2003). Lastly, the use of rapid production machines like SLM will mitigate labor and human error, and the additive manufacturing process eliminates the need for multipart design, machining and assembly. Since the design files are adopted from the solid model of the part, the use of digital files can take out a large amount of human error because the

engineer will not need to interpret drawings and make the part, because the design file is simply loaded from the 3D model (David, 2014).

Additive manufacturing, or the SLM process in particular, offers the possibility for producing ready to use metal parts. These parts can be ready to use with minimal post processing. For instance, parts made from additive manufacturing can be seen in products such as NASA's new J-2x rocket engine (Hewitt, 2012). Additive manufacturing machines offer the capability to produce one off pieces that can be quickly adjusted on the fly in remote locations that may not have access to other manufacturing methods. Additionally, additive manufacturing produces parts in a compact manner without requiring the designed to break the design into multiple components due to manufacturing constraints. The SLM process produces parts that are completely homogenous with a consistent structural integrity and without leaving any weak points on the manufactured part that may lead to failure.

Additive manufacturing technology, and SLM technology in particular, offers a robust alternative that can be useful in many industries. The current literature refers to multiple research efforts that are attempting to improve the technology even further. As SLM advances, it can be stated that it will be used more and more due to its ability to produce an exact part wherever and whenever it is needed. It can significantly reduce the time spent in the early phases of product development since any questions with regards to shape, fit, compatibility, etc. can be quickly answered without requiring the team to go through a long period of manufacturing. Parts can be designed, redesigned and easily modified by printing them iteratively as the design cycle progresses. The current issues with the additive manufacturing technology such as long build time, difficulty in removing support material, and high cost can be potentially overcome as more research is done in the field of processes such as SLM.

2.3.2 Current Technology

Most of the current research focus in 3D printing of metals has been on the use and improvement of the SLM process. This process uses high intensity lasers to create a larger melt pool of the material when the powder material is heated. This larger melt pool penetrates through multiple layers to bind together more material with each pass rather than binding each particle to the next, as seen with the SLS process (Noe, 2014). This creation of a larger melt pool is seen to be significantly advantageous in increasing the density of the part and resulting in strength properties that are similar to conventional manufacturing. During the post processing of the material, a functional part can be normalized in a heat treating furnace, thereby removing any residual stresses accumulated within the part during manufacturing (Casalino, 2014).

Currently there are a number of manufacturers who are producing SLM printers. These include 3D Systems, SLM Solutions, and Electro Optical Systems (or EOS). The recently released EOS M290 is considered to be the state of the art in the market. The M290 printer has a significantly easier interface than the other SLM machines currently in the market. The M290 printer is not a block box, and has an array of enhanced monitoring systems that allow the user to manage quality to the highest degree and customize the build to some extent. The new monitoring system includes an improved gas management system, a new software that is more intuitive, etc. This machine offers a build area of 250mm x 250mm x 325mm. This is not the largest build area currently available, but provides enough space to produce medium size parts. One major advantage of this machine, and the SLM process in general, is the ability to process a multitude of metals and alloys. EOS offers 13 proprietary alloys that can be used for production. These alloys include steel, aluminum, cobalt chrome, nickel, and titanium. Other materials that have been used in similar processes include copper, and even some quasicrystals (Dai, 2014,

Quasicrystals, 2014). Overall, the current state of this technology is rapidly evolving and making it possible to move from the prototype phase to the production phase very rapidly.

2.4 Summary

This chapter discusses the literature study conducted for this research. Additive manufacturing is an exciting technology that has been rapidly evolving over the last decade. The most important aspect of investigation in the use of SLM for manufacturing parts is to determine whether parts will have the capability to withstand static and dynamic loads, similar to conventional manufacturing methods. The purpose of this research is to investigate the dynamic properties of parts made by the SLM process. Specifically, dynamic properties of cantilever beams are evaluated by using a laser vibrometer and identifying the natural frequencies and mode shapes. These properties are directly compared with beams that are manufactured through conventional methods (such as rolling). Other tests such as tensile testing and hardness testing are performed to also relate the results of static testing to dynamic testing. Parts made from the SLM process are manufactured at a few different settings to investigate the influence of process parameters on the overall dynamic properties. The vibrometer data is post processed and compared in the form of frequency response. The theoretical model developed for this study is discussed in Chapter 3. The experimental set up, data collection and the results are presented in Chapter 4. The overall conclusions and future scope are discussed in Chapter 5.

CHAPTER 3: MATHEMATICAL MODELING

This chapter presents the mathematical model that has been used for this study. The main purpose of this model is to have a reference that can be used to compare the experimental results. Some of the computational tools that have been used during this study are also discussed in this chapter.

3.1 Beam Modeling

The mathematical model has been created by using the geometrical and material properties of the beam. First, using the geometry of the beam, the area moment of inertia, section modulus and equivalent stiffness were calculated, as seen below:

$$I = (w * h^2)/12 \quad (3.1)$$

$$Z = (w * h^2)/6 \quad (3.2)$$

$$K = (3 * E * I)/l \quad (3.3)$$

In Eqs. (3.1), (3.2) and (3.3), w and h are the width and height of the beam cross-section, l is the length of the beam, E is the modulus of elasticity and I is the area moment of inertia.

For the first model an equivalent mass and an equivalent stiffness were used. This equivalent mass for a cantilever beam can be calculated using $.23 * mass$ (Rao, 2011), and simulates a lumped mass concentrated at the end of the beam rather than being distributed across the length of the beam. The material constants used for 316L stainless steel include the modulus of elasticity of 193 GPa, and a density of 7.9 g/cm^3 .

The mathematical model first calculated deflection for a cantilever beam, like the set up that was used for testing. This section of the program seen below in Figure 3.1 uses a loop to calculate deflections at multiple points across the beam and then plots the deflection of each individual point.

```
for X = 0:N:Length
    Deflection=((Force*X^2)/(6*E*I))*(3*Length-X);
    def=[def,Deflection];
end

figure(1)
plot(points,def)
title('bending beam')
grid on
xlabel('length (m)')
ylabel('Deflection (m)')
```

Figure3. 1 Static Deflection Model.

This section of the code calculates the maximum value of deflection for a specific point load acting upon the beam. After the loop has finished running the individual deflection values can be pulled out of the output array. With the forces acting on the end of the beam, the greatest deflection in a cantilever beam occurs at the tip of the beam. Below, Figure 3.2 shows the plot of this deflection using a static load of 10 N.

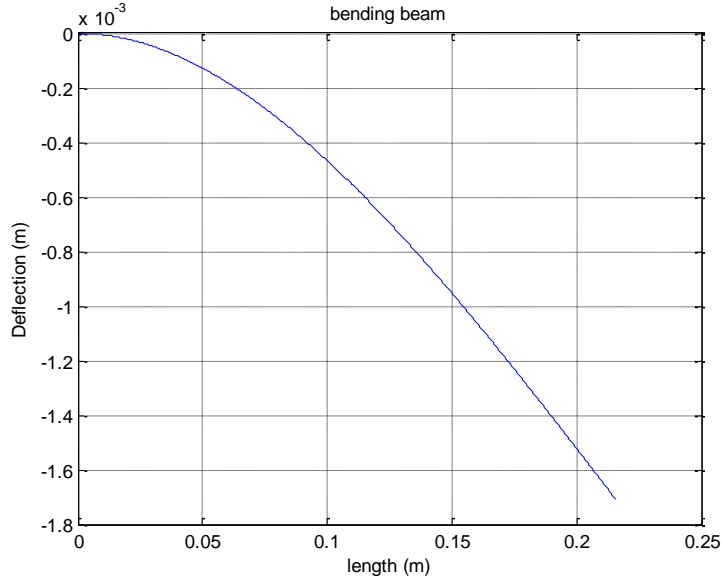


Figure 3.2 Bending Deflection – static load.

It may be noted that the code used for calculation can be adjusted to accept any geometry and material parameters and give an accurate result of the deflection of a cantilever beam that can be expected under a given static point load.

The first three bending mode shapes and natural frequencies are calculated using the beam model. The Euler-Bernoulli governing equation of motion (EOM) for a beam with a constant area of cross-section, A , and a time varying force acting on the beam can be expressed as follows:

$$\rho A \frac{\partial^2 y(x,t)}{\partial t^2} + EI \frac{\partial^4 y(x,t)}{\partial x^4} = f_s(x, t) \quad (3.4)$$

In Eq. (3.4), E is the modulus of elasticity of the beam material, ρ is the density of the beam material and I is the area moment of inertia of the cross-section; $y(x,t)$ is the transverse displacement of the beam and $f_s(x,t)$ is the time varying force per unit length acting on the beam.

Using the homogeneous or free vibration form of Eq. (3.4) and using separation of variables, with

$c^2 = \frac{EI}{\rho A}$, $y(x, t) = X(x)T(t)$ and $\beta^4 = \frac{\omega^2}{c^2} = \frac{\rho A \omega^2}{EI}$, yields two separate solutions as:

$$X(x) = C \cos\beta x + D \sin\beta x + E \cosh\beta x + F \sinh\beta x \quad (3.5)$$

$$T(t) = A \cos\omega t + B \sin\omega t \quad (3.6)$$

In Eqs. (3.5) and (3.6), C, D, E, F are constants that can be determined from the substitution of the boundary conditions, and A, B are constants that can be determined from the substitution of the initial conditions. As a result the mode shapes corresponding to each natural frequency can be determined as:

$$X(x) = c_1 \cos\beta x + c_2 \sin\beta x + c_3 \cosh\beta x + c_4 \sinh\beta x \quad (3.7)$$

In Eq. (3.7), c_1, c_2, c_3, c_4 are constants that can be determined by using the boundary conditions of the cantilever beam. The mode shapes can be found corresponding to each natural frequency:

$$\omega_n = (\beta_n l)^2 \sqrt{\frac{EI}{\rho A l^4}} \quad (3.8)$$

For a cantilever beam, the corresponding values are as follows: $\beta_1 l = 1.875104$, $\beta_2 l = 4.694091$, $\beta_3 l = 7.854757$.

Figure 3.3 shows the section of the MATLAB program that calculates the mode shapes. In this section, beam equations are used to calculate the first three mode shapes across the length of the beam.

```

108 %Cantilever MODE SHAPES
109 - beta1=(1.875104/Length);
110 - beta2=(4.694091/Length);
111 - beta3=(7.854757/Length);
112 - alpha1=( (sin(beta1*Length)+sinh(beta1*Length)) / (cos(beta1*Length)+cosh(beta1*Length)) );
113 - alpha2=( (sin(beta2*Length)+sinh(beta2*Length)) / (cos(beta2*Length)+cosh(beta2*Length)) );
114 - alpha3=( (sin(beta3*Length)+sinh(beta3*Length)) / (cos(beta3*Length)+cosh(beta3*Length)) );
115
116 mode1=[];
117 mode2=[];
118 mode3=[];
119 - for x=0:N:Length
120
121 -     y1=(sin(beta1*x)-sinh(beta1*x)-alpha1*(cos(beta1*x)-cosh(beta1*x)));
122 -     y2=(sin(beta2*x)-sinh(beta2*x)-alpha2*(cos(beta2*x)-cosh(beta2*x)));
123 -     y3=(sin(beta3*x)-sinh(beta3*x)-alpha3*(cos(beta3*x)-cosh(beta3*x)));
124
125 -     mode1=[mode1,y1];
126 -     mode2=[mode2,y2];
127 -     mode3=[mode3,y3];
128
129 - end

```

Figure 3.3 Mode Shape Model.

The first three (bending) natural frequencies are computed and the corresponding mode shapes are plotted to establish a baseline for the experimental results. Figure 3.4 shows the model used for computing the natural frequencies from the continuous model of the beam.

```

%Frequency response SIMPLIFIED Equivalent Mass
zeta=.01;
C=zeta*sqrt(2*Mass*K);
transfer=[];
W=0:0.1:1200;
for w = W
    Trans=(1/((-Mass*w^2)+(j)*C*w)+K) ;
    transfer=[transfer,Trans] ;
end
freq1=((1.875014)^2)*sqrt((E*I)/(Mass1*Length^3))/(2*pi)
freq2=((4.694091)^2)*sqrt((E*I)/(Mass1*Length^3))/(2*pi)
freq3=((7.854757)^2)*sqrt((E*I)/(Mass1*Length^3))/(2*pi)

```

Figure 3.4 Equivalent frequency response.

The frequency response of the cantilever beam can be calculated as the ratio of displacement to a sinusoidal input force with varying frequency. A MATLAB program has been

generated to plot the full frequency response for the model of the beam discussed above. Figure 3.5 shows the program for calculating this response. This response will result in peaks corresponding to the natural frequencies of the beam. This simulation does not take into account the higher degrees of freedom or the axial and torsional frequencies, but is limited to the frequencies corresponding to the bending modes. The experimental results, however, will not be limited to the bending modes, and may demonstrate torsional or axial modes as well.

```

%Full Cantilever Frequency response
TL=Length ; %test location
X1=(sin(beta1*Length)-sinh(beta1*Length))-alpha1*(cos(beta1*Length)-cosh(beta1*Length));
X2=(sin(beta2*Length)-sinh(beta2*Length))-alpha2*(cos(beta2*Length)-cosh(beta2*Length));
X3=(sin(beta3*Length)-sinh(beta3*Length))-alpha3*(cos(beta3*Length)-cosh(beta3*Length));
Xs1=(sin(beta1*TL)-sinh(beta1*TL))-alpha1*(cos(beta1*TL)-cosh(beta1*TL));
Xs2=(sin(beta2*TL)-sinh(beta2*TL))-alpha2*(cos(beta2*TL)-cosh(beta2*TL));
Xs3=(sin(beta3*TL)-sinh(beta3*TL))-alpha3*(cos(beta3*TL)-cosh(beta3*TL));

FFT=[];
for w = W
    H1=1/((freq1^2)-(w^2)+2*xi*w*freq1*zeta);
    H2=1/((freq2^2)-(w^2)+2*xi*w*freq2*zeta);
    H3=1/((freq3^2)-(w^2)+2*xi*w*freq3*zeta);

    freq_response = (1/(density*(Height*Width)))*((X1*(Xs1)*H1*w)+(X2*(Xs2)*H2*w)+(X3*(Xs3)*H3*w));
    FFT=[FFT,freq_response];
end

```

Figure 3.5 Calculation of frequency response.

The complete MATLAB programs developed for mathematical modeling and analysis for this study are presented in the Appendix.

3.2 Results

This section shows all the results from the mathematical model. These results are summarized and briefly discussed in this section.

3.2.1 Frequency Response

The frequency response plot generated from the mathematical model clearly displays the peaks corresponding to the natural frequencies and should correlate to the results from dynamic testing. The results can be seen in Figure 3.6, the peaks in the frequency response plot show the expected first three bending modes. Multiple cantilever beams manufactured through two

different methods will be tested. The frequency response of the tested beams will be directly compared to the response in Figure 3.6. Developing a mathematical model is important since it provides a reference that can be used before finalizing the test set up with the laser vibrometer. The mathematical model provides the expected behavior of the system so that the results can be directly compared to make sure that the test is being set up correctly and adequately with appropriate boundary conditions, excitation input, etc.

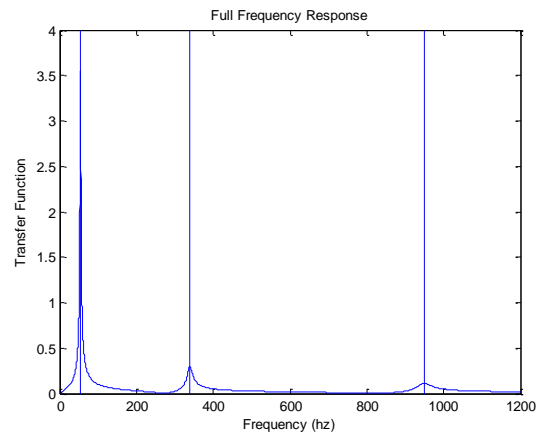


Figure 3.6 Frequency response – cantilever beam.

3.2.2 Natural frequencies and mode shapes

The first three bending modes and the corresponding natural frequencies of the system, as calculated from the model are shown in Figures 3.7, 3.8 and 3.9. These mode shapes are characterized by the number of nodes in the mode shape across the length of the beam. The first bending mode does not have any nodes whereas the other two modes have one or two nodes respectively.

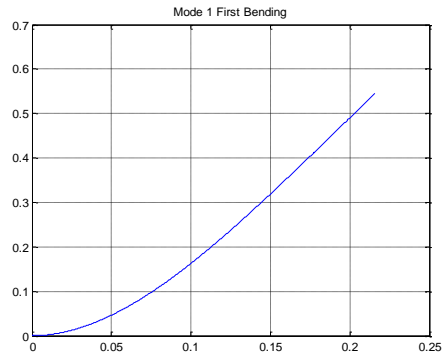


Figure 3.7 First Mode Shape (Bending).

It may be noted that the mode shapes are plotted across the length of the beam, therefore the x-axis of the beam corresponds to the length of the beam varying from 0 to 0.25 m

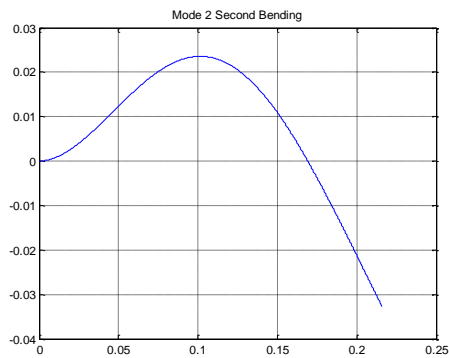


Figure 3.8 Second Mode Shape (Bending).

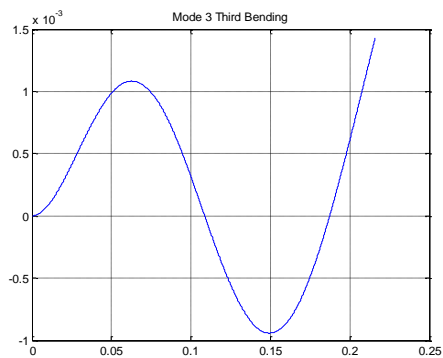


Figure 3.9 Third Mode Shape (Bending).

The three mode shapes shown above correspond to the calculated natural frequencies. Table 3.1 shows these calculated natural frequencies. The mathematical model estimates that these frequencies will be at 54.07 Hz, 338.90 Hz and 948.93 Hz. The cantilever beam will exhibit the bending mode shapes in Figures 3.7, 3.8 and 3.9 at these three frequencies.

Table 3.1 Calculated Natural Frequencies

Calculated Natural Frequencies	
1st Frequency (Hz)	54.0723
2nd Frequency (Hz)	338.9036
3rd Frequency(Hz)	948.9399

3.3 Summary

This chapter presented the mathematical model that has been developed in this study. The mathematical model is an important step to establish a reference for dynamic testing. This model makes it possible to understand the expected results and diagnose any problems in the test set up that may come up while conducting complex testing. When noise is introduced to the system in the real world testing, it can be challenging to reliably conclude whether the results are correct or not. A robust mathematical model is extremely useful to make sense of the data and to aid in the understanding the measured output. The mathematical model has been used to calculate the frequency response, the natural frequencies and the mode shapes of the cantilever beam. These results will be compared to the results from the experiment in the next chapter.

CHAPTER 4: EXPERIMENTAL RESULTS

This chapter briefly discusses the equipment used for testing during this research. This is followed by the experimental results obtained from testing. Some discussion on the post-processed results is also included in this chapter.

4.1 Test Equipment

This section provides an overview of the equipment and machinery that have been used for the purpose of this research. Figure 4.1 shows the SLM printer used for manufacturing the parts. This machine (EOS M290) is the state-of-the-art that is currently used in the industry.

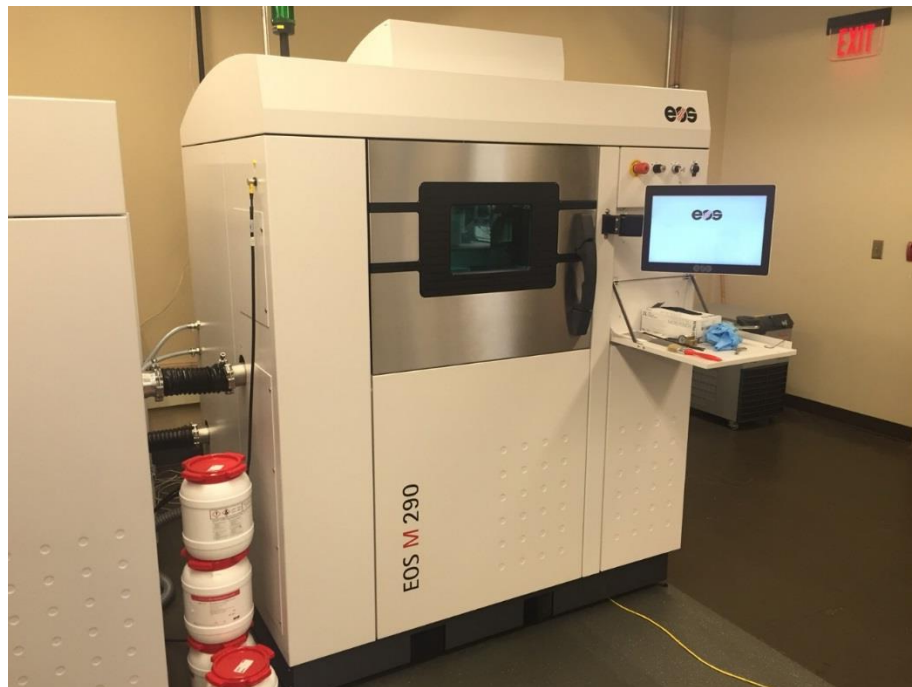


Figure 4. 1: EOS M290 SLM 3D Printer.

Figure 4.2 shows the Instron® 5967 tensile testing machine that was used to test the static properties of the samples made by traditional manufacturing as well as additive manufacturing. This test equipment has been used to determine the stress-strain curve, that is used to find the yield and ultimate strengths of the materials as well as the modulus of elasticity. The stress-strain

curve is calculated from the load-deflection data that is reported by the data acquisition connected to the tensile tester.



Figure 4.2: Instron 5967 Tensile Tester.

Figure 4.3 shows the laser vibrometer that has been used for dynamic testing in this research. This equipment is used to measure the velocities of the test sample by using a laser and the Doppler effect to determine the displacement and velocity of the part that is excited at various frequencies. This is a non-contact method and is advantageous as compared to the use of an accelerometer since the test part does not need to be modified in any way. The vibrometer has

its own data acquisition system that can be used to collect the velocity data and process the data to get the frequency response and visualize the mode shapes.



Figure 4.3: Polytec PSV-400 Scanning Laser Vibrometer.

The main specifications of the equipment discussed in this section can be found in the Appendix for reference.

4.2 Experimental Setup – Static Testing

To conduct the static testing dog bone coupons were printed on the EOS m290, as well as cut using a laser cutter from cold rolled steel. These coupons were designed to the ANSI E8 standards for tensile coupons. These coupons were tested using the Intron 5967 tensile tester. This system pulls the coupons and measures the load and deflection experienced by the part until

failure. Once the load and deflection data is collected this can be used to calculate the ultimate tensile stress as well as the elastic modulus for the material.

4.3 Experimental Setup – Dynamic Testing

To conduct the dynamic testing, multiple beams were printed on the EOS M290 Direct Metal Laser Sintering system (DMLS). These beams were produced using four different settings of the DMLS system. The parameters of layer thickness and number of scans of each layer were selected as the primary variables of interest. These parameters were selected because of their potential effect on the parts manufactured with the DMLS system. The thickness of the build layer is important because by increasing the thickness (of each layer) from 20 to 30 microns, 50% of the layers can be removed and this can significantly decrease the build time for manufacturing a part. Secondly, the number of scans for each layer was selected as a variable of interest. This parameter was varied by two levels, including a single and double scan. Double scanning was selected because scanning the layer twice should increase the density of the manufactured part and assist in normalizing the part during the build process (Yasa, 2011). The first set of parts were produced by using the base parameters for 316L Stainless Steel (SS). This setting scans each layer once and builds with layers of 20 micron thickness. Parts were also produced by using a single scan with a layer thickness of 20 microns, a single scan with a layer thickness of 30 microns, and a double scan with a layer thickness of 30 microns. All the parts were tested by using the Polytech PSV-400 laser vibrometer to determine the mode shapes, natural frequencies and the damping ratios corresponding to each mode. The line diagram for the test setup is shown in Figure 4.4.

The laser vibrometer uses the Doppler Effect to measure the velocity at a specific location on a part. As can be seen in Figure 4.4, the laser vibrometer splits the beam into two

signals. One of these beams is the reference beam and the other is projected onto the surface of the test piece. The light then reflects back to the scan head and is compared to the signal from the reference beam. The backscattered light reflecting from the surface of the part is phase shifted based on the vibration within the part. This Doppler shift is proportional to the velocity of the test sample, approximately 1 m/s of vibration represents close to 3.16 MHz of shift in the light's frequency. Figure 4.5 shows a picture of the test setup and Figure 4.6 shows the scan grid of a beam that was tested during this research.

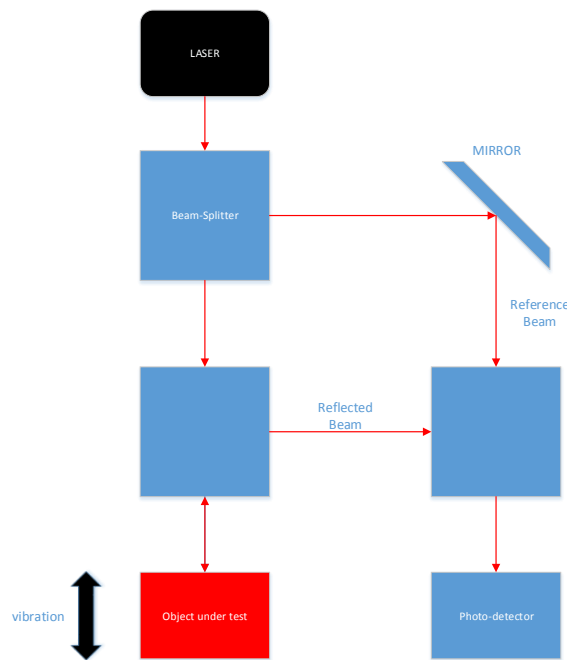


Figure 4.4 Vibrometer Test Layout.



Figure 4.5 Picture of Test Setup.

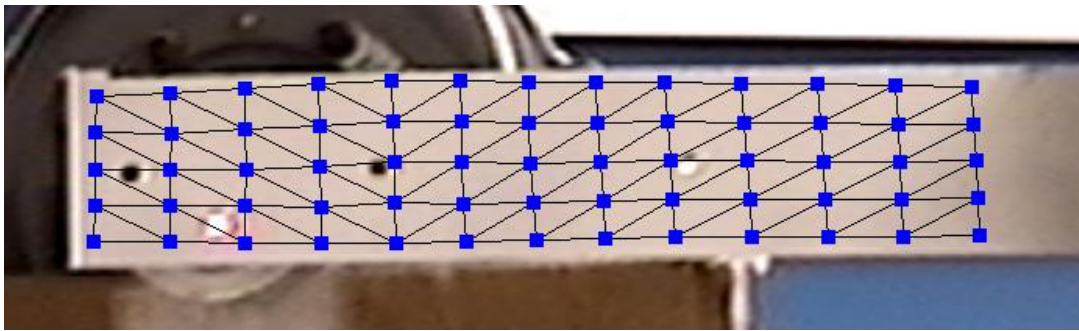


Figure 4.6 Scan Grid of the beam.

A cantilever beam configuration was used for dynamic testing since this is a generic part without a complicated geometry. Also, this geometry is commonly used in mechanical and civil structures. A fixture was designed to hold the beam at a 90 degree angle and at a distance of 1 m from the scan head, as seen in Figure 4.5. Two excitation inputs were used, however the acoustics excitation input was found to be more consistent. The signal generator built into the Polytech system was used to generate this acoustic signal. The signal created a periodic chirp covering a frequency range of 100-2000 Hz. This range covered the expected natural frequencies of the beam geometry. A grid is created across the part surface, one such example (13 x 5 grid) is

shown in Figure 4.6. This grid defines the scan points for the laser vibrometer. Each point was scanned a total of 25 times. These 25 scans are averaged together, and then each of the averaged points is combined to create the average spectrum for the tested part.

4.4 Results – Static Testing

Static properties of the materials were tested by using the (Instron) tensile testing machine. Dog bone coupons were used for testing since these coupons are a standard for tensile testing. One set of parts was manufactured by using the laser cutter (traditional manufacturing), the material was purchased off the shelf and was rolled. The second set of parts was manufactured (printed) with the DMLS system. All parts were made from 316L Stainless Steel. The printed coupons were produced using the single scan setting with a layer thickness of 20 microns. This is the default parameter set for the EOS M290 system. These dog bone coupons were built as per the E8 standard (from ASTM) for test coupons. (ASTM, 2013) These coupons were tested in extension at the same strain rate and the results from this test are summarized in Table 4.1. The results in Table 4.1 show the maximum force held by each coupon, the calculated ultimate tensile stress and the modulus of elasticity of each part.

Table 4.1 Tensile Test – Results.

Material	Sample	Max Load (N)	Tensile Stress (Mpa)	Modulus (N/mm)
Printed	1	8390.38	559.3586667	3854.8
	2	8416.253	561.0835333	3830.2
	3	8353.002	556.8668	3946.1
	4	8366.696	557.7797333	3829.6
	5	8375.175	558.345	3785.3
	6	8389.605	559.307	3771.1
	7	8352.892	556.8594667	3743.7
	8	8434.642	562.3094667	3858.5
	9	8408.847	560.5898	3847.4
	10	8433.701	562.2467333	3870
Laser Cut	1	5234.791	545.2907292	2992.8
	2	5253.349	547.2238542	3197
	3	5197.02	541.35625	3048.9
	4	5081.547	529.3278125	3051.9
	5	5080.2	529.1875	3025.5
	6	5113.699	532.6769792	2982
	7	4763.138	496.1602083	3372.6
	8	5061.445	527.2338542	3035.7
	9	5242.174	546.0597917	3053.7
	10	5050.073	526.0492708	2940

Table 4.2 shows the average values – for the printed parts and for the parts that were manufactured by a laser cutter. A t-test has been conducted to determine whether there is any statistically significant difference between the static properties of the parts. The ultimate tensile stress and the modulus of elasticity are compared and the results of these t-tests can be seen in Tables 4.3 and 4.4.

Table 4.2 Comparison – Averages.

	Max Load (N)	Tensile Stress (Mpa)	Elastic Modulus (MPa)
Printed	8392.1193	559.47462	3833.67
Laser Cut	5107.7436	532.056625	3070.01

Table 4.3 Results – t-test – Ultimate Tensile Stress.

	<i>Engg. Stress PRINTED (MPa)</i>	<i>Max Stress CUT (MPa)</i>
Mean	559.47462	532.056625
Variance	4.153685823	227.9690381
Observations	10	10
Hypothesized Mean Difference	0	
df	9	
t Stat	5.690846399	
P(T<=t) one-tail	0.000148871	
t Critical one-tail	1.833112933	
P(T<=t) two-tail	0.000297742	
t Critical two-tail	2.262157163	

Table 4.4 Results – t-test – Elastic Modulus.

	<i>Elastic Modulus (MPa) PRINTED</i>	<i>Elastic Modulus (MPa) CUT</i>
Mean	3833.67	3070.01
Variance	3287.751222	15832.761
Observations	10	10
Hypothesized Mean Difference	0	
df	13	
t Stat	17.46426376	
P(T<=t) one-tail	1.043E-10	
t Critical one-tail	1.770933396	
P(T<=t) two-tail	2.08599E-10	
t Critical two-tail	2.160368656	

After reviewing the results of the t-tests from Tables 4.3 and 4.4, it can be concluded that there is some statistically significant difference between the two sets for both the ultimate tensile stress and the elastic modulus. For the printed samples, the average ultimate tensile stress is found to be higher than that of the parts manufactured by laser cutting the rolled sheet of 316L Stainless Steel. The elastic modulus for the printed samples was also found to be significantly higher. These results indicate that parts manufactured by the Selective Laser Melting process are equivalent or better than parts manufactured from traditional means of manufacturing in terms of properties associated with static loading, such as strength (ultimate tensile strength) and stiffness (modulus of elasticity). This is an important result and implies that Selective Laser Melting can

be used to substitute traditional means of manufacture. However, it may be noted that the process parameters such as build layer thickness, laser intensity, number of scans, etc. need to be carefully considered.

4.5 Results – Dynamic Testing

Dynamic testing of the test samples was carried out by using the Polytech PSV-400 scanning laser vibrometer described in Section 4.1. Table 4.5 shows a description of the multiple parameters used for making the samples for dynamic testing. Parts were manufactured by using a single scan or a double scan with a layer thickness of 20 microns or 30 microns. Table 4.6 shows the list of natural frequencies, second through sixth, for each sample that was used for this test. Due to problems with the excitation and consistent measurement, it was very challenging to consistently measure the first frequency. Therefore, the first frequency is not being reported in Table 4.5. A relatively small excitation device would be required to operate at low frequencies in order to successfully measure the first frequency. All the frequency response plots are superposed in one plot, as shown in Figure 4.7. All five natural frequencies can be detected from the frequency response. Zooming into the frequency range of interest will clearly demonstrate the peaks corresponding to each frequency. Since the frequency response in Figure 4.7 is pretty dense, portions of the response have been separately shown in the Appendix. A couple of these zoomed plots for the second and third frequency are shown in Figures 4.8 and 4.9. The frequency response indicates that the peaks and the natural frequencies are repeatable, as seen in the results summarized in Table 4.6.

Table 4.5 Build Parameter Legend

Legend	Number of scans	layer thickness
SS20	Single Scan	20 Micron
SS30	Single Scan	30 Micron
DS20	Double Scan	20 Micron
DS30	Double scan	30 Micron
Water Jet	Cold Rolled 316L Stainless Steel	

Table 4.6 Natural Frequency Results.

2nd Frequency (Hz)	1	2	3	4	5	average
SS20	296.875	298.5625	301.5	303.13	302.5	300.5135
SS30	310.1419	312.1875	309.1875	310.3175	308.875	310.1419
DS20	309.875	308.25	305.625	308.8125	308.1875	308.15
DS30	307.5625	304.875	305.0025	307.25	300.94	305.126
Water Jet	313.5	315.8125	315.875	319.4375	320.1875	316.9625
3rd Frequency (Hz)	1	2	3	4	5	average
SS20	534.8125	536.1875	554.6875	556.8125	555.5	547.6
SS30	553.875	553.5	550.8125	552.1925	550	552.076
DS20	548.625	550.1875	545.25	549.8125	550.125	548.8
DS30	554.875	553.125	550.0025	553.8125	554.06	553.175
Water Jet	545.5	548.0625	544.5	546.875	547.5	546.4875
4th Frequency (Hz)	1	2	3	4	5	average
SS20	788	792.125	802.4375	805.8125	802.8125	798.2375
SS30	823.5	825.9375	816.5	820.63	817.375	820.7885
DS20	818.9375	815.5	805.9375	820.3125	815.0625	815.15
DS30	813.1875	806.0625	800.0025	811.0625	789.6925	804.0015
Water Jet	833.75	843.125	841.5625	845.375	846.1875	842
5th Frequency (Hz)	1	2	3	4	5	average
SS20	1437.5	1451.1	1496.2	1472.55	1505.4	1472.55
SS30	1544.9	1546.1	1533.8	1542.8	1532.5	1540.02
DS20	1528.1	1531.8	1513.1	1534.5	1531.1	1527.72
DS30	1511.3	1517.3	1515	1523.2	1489.7	1511.3
Water Jet	1551.5	1535.9	1551.3	1579.3	1554.5	1554.5
6th Frequency (Hz)	1	2	3	4	5	average
SS20	1637.1	1641.8	1691.1	1700.8	1697.4	1673.64
SS30	1695.8	1694.1	1686.4	1688.8	1686.3	1690.28
DS20	1679.2	1677.8	1665.6	1679.4	1677.8	1675.96
DS30	1690.4	1683.8	1675.3	1690.4	1660	1679.98
Water Jet	1679.9	1676.6	1667.9	1676.1	1676.4	1675.38

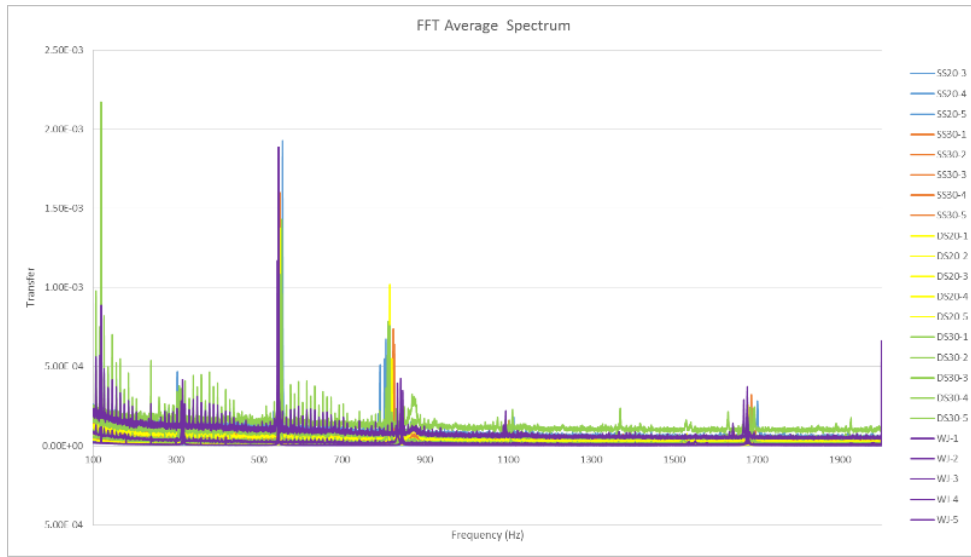


Figure 4.7 Frequency response.

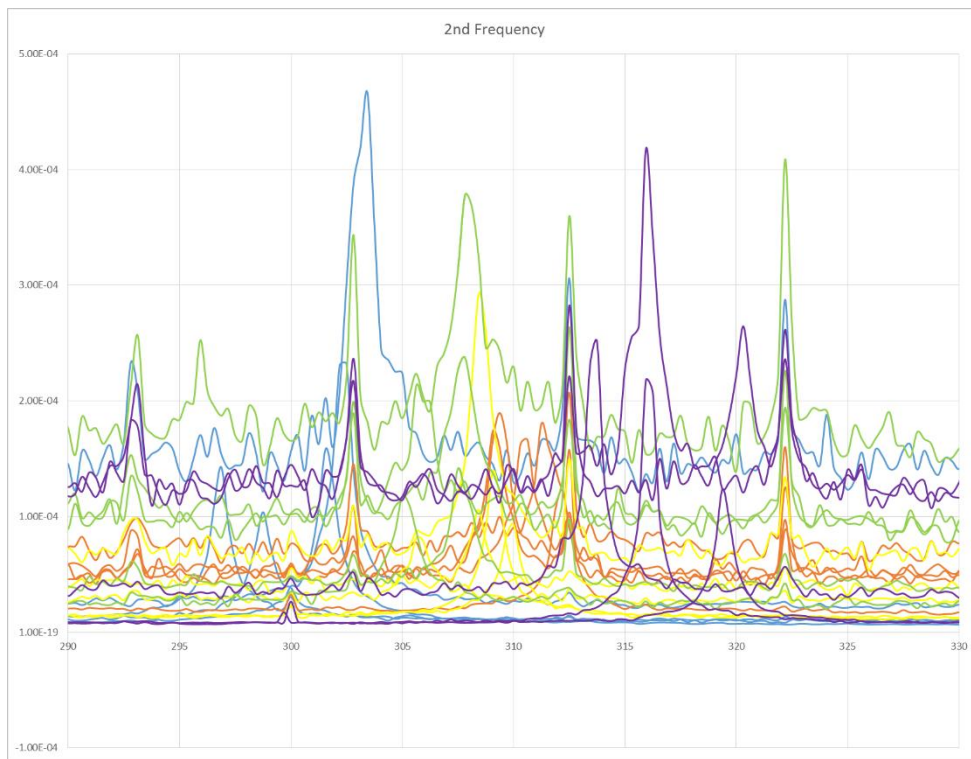


Figure 4.8 Frequency response – around second frequency.

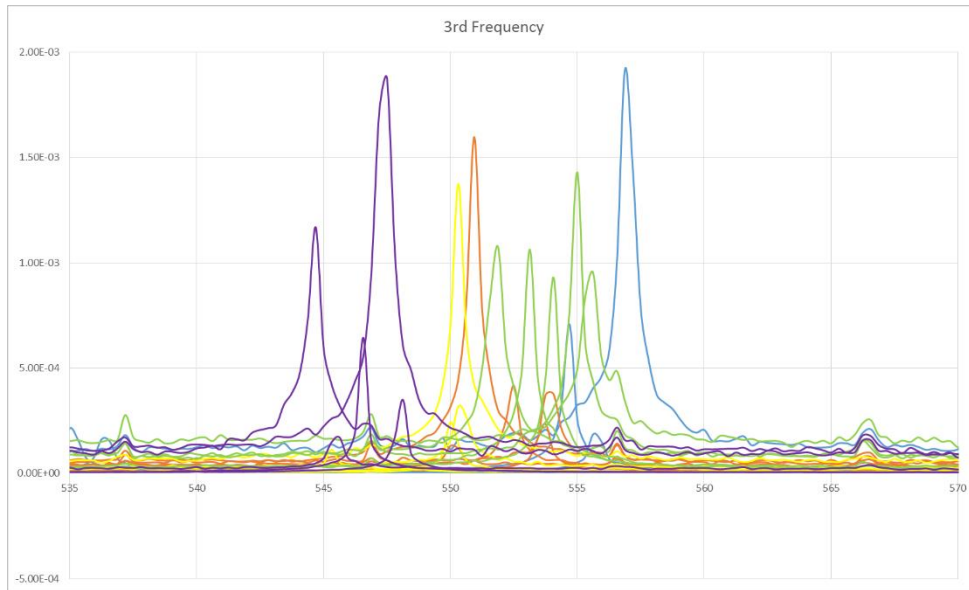


Figure 4.9 Frequency response – around third frequency.

The frequency response has also been used to calculate the damping ratios corresponding to each natural mode. These values are calculated by using the peaks corresponding to each natural mode and can be seen in Table 4.7. The calculation of the damping ratios has been based on detecting the half power points and the bandwidth for each mode from the frequency response. The Matlab program used for this calculation has been included in the Appendix. All the damping ratios are seen to be well below 1, implying that each test sample is underdamped, as expected.

Table 4.7 Damping Results.

Damping Ratio 2	1	2	3	4	5	average
SS20	0.0011	0.001	0.001	0.001	0.001	0.00102
SS30	0.001	0.001	0.001	0.001	0.001	0.001
DS20	0.001	0.001	0.001	0.001	0.001	0.001
DS30	0.001	0.001	0.001	0.001	0.001	0.001
Water Jet	0.000997	0.00099	0.000989	0.000978	0.000976	0.000986
Damping Ratio 3	1	2	3	4	5	average
SS20	0.000584	0.000583	0.000563	0.000561	0.000563	0.000571
SS30	0.000564	0.000565	0.000567	0.000566	0.000568	0.000566
DS20	0.000382	0.000383	0.000388	0.000381	0.000383	0.000383
DS30	0.000563	0.000565	0.000568	0.000564	0.000574	0.000567
Water Jet	0.000573	0.00057	0.000574	0.000571	0.000571	0.000572
Damping Ratio 4	1	2	3	4	5	average
SS20	0.000397	0.000395	0.000389	0.000388	0.000389	0.000392
SS30	0.000379	0.000378	0.000383	0.000381	0.000382	0.000381
DS20	0.000382	0.000383	0.000388	0.000381	0.000383	0.000383
DS30	0.000384	0.000388	0.000391	0.000385	0.000396	0.000389
Water Jet	0.000375	0.000371	0.000371	0.00037	0.000369	0.000371
Damping Ratio 5	1	2	3	4	5	average
SS20	0.000217	0.000215	0.000209	0.000212	0.000208	0.000212
SS30	0.000202	0.000202	0.000204	0.000203	0.000204	0.000203
DS20	0.000205	0.000204	0.000207	0.000204	0.000204	0.000205
DS30	0.000207	0.000206	0.000206	0.000205	0.00021	0.000207
Water Jet	0.000201	0.000203	0.000201	0.000198	0.000201	0.000201
Damping Ratio 6	1	2	3	4	5	average
SS20	0.000191	0.00019	0.000185	0.000184	0.000184	0.000187
SS30	0.000184	0.000184	0.000185	0.000185	0.000185	0.000185
DS20	0.000186	0.000186	0.000188	0.000188	0.000186	0.000187
DS30	0.000185	0.000186	0.000187	0.000185	0.000188	0.000186
Water Jet	0.000186	0.000186	0.000187	0.000186	0.000186	0.000187

Some of the observations from the natural frequency results in Table 4.6 are as follows: the natural frequency increases for parts made using the double scanning method as compared to the single scan (with the layer thickness remaining the same), this increase is seen to range from 0.5% to 3.5%; the increase in natural frequency is not observed if the layer thickness is higher (30 microns in the case of this study); the natural frequency of the samples is comparable to rolled parts made by water jet cutting, however the parameters (layer thickness and number of scans) need to be judiciously selected.

The damping results from Table 4.7 indicate that the damping ratios of the printed parts are slightly higher than the rolled parts. This is seen to be regardless of the parameters used in

the Selective Laser Melting process. This could provide an advantage and will need to be investigated further.

4.6 Summary

The results from static testing indicate that the strength and stiffness of the parts made by the Selective Laser Melting process is equivalent (or better) to parts made from conventional manufacturing methods such as rolling. The results from dynamic testing, however, indicate that process parameters play an important role in determining the natural frequencies and damping ratios. This could be possibly attributed to the density of the parts varying significantly with process parameters, and generally reported to be around 97% of the parts manufactured through processes such as forging, casting, rolling, etc. (Swift, 2013). The results from dynamic testing presented in this chapter can be used to directly compare the fatigue behavior of the parts manufactured through two distinct processes. The damping ratios, natural frequencies and frequency response can be used to qualitatively predict fatigue behavior, as has been reported in existing research literature (Damir, 2007).

CHAPTER 5: CONCLUSIONS AND FUTURE RESEARCH

The rapid development of digital manufacturing and additive manufacturing processes over the last two decades has generated a lot of excitement among the design, development and manufacturing professionals. While traditional processes such as forging, casting, rolling, etc. require a long lead time in the development of tooling, the transition from a three dimensional model to an end product is seen to be significantly shorter through the use of additive manufacturing. However, there are multiple questions that need to be answered before an additive manufacturing process such as Selective Laser Melting (SLM) can become widespread. This study examined some aspects of parts manufactured by the SLM process, particularly properties associated with the dynamic response.

5.1 Conclusions

The results from static testing indicate that the strength and stiffness properties of parts manufactured through the SLM process is statistically equivalent to or better than other parts made by laser cutting cold rolled stock material. The static testing shows that the parts produced through SLM are slightly stiffer in the longitudinal direction than the other parts. This conclusion is simply based on comparing the modulus of elasticity of the ten parts that were made through each process and tested on the tensile testing machine.

The dynamic testing is seen to point to some significant differences between parts made through additive manufacturing and the SLM process and the parts made through conventional subtractive manufacturing processes. Multiple cantilever beams were used for dynamic testing and the dynamic response of the beams was measured by a vibrometer connected to a data acquisition system. Two process parameters associated with the SLM process also indicate an

influence over dynamic properties. The testing in this study was limited to 316L stainless steel, therefore all conclusions are based on this material only.

It is observed that the damping ratios of all the parts made by the SLM process are relatively higher for all the bending modes. The damping ratios corresponding to the torsional modes do not show a clear trend. For an underdamped system, this is a significant result and implies that the bending modes will exhibit relatively lower damping peaks, thereby significantly influencing the fatigue life of these parts. Also, it is observed that the process parameters, number of scans and the layer thickness do not exhibit a significant influence on the damping ratio. It should, however, be noted that only two levels of these two parameters were investigated in this study. The number of scans was limited to one or two whereas the layer thickness was limited to 20 microns or 30 microns.

On the contrary, process parameters seem to significantly affect the natural frequencies. It is observed that the natural frequencies of all parts made by the SLM process are lower than the other parts, regardless of the process parameters. However, double scan seems to increase natural frequency, particularly for the lower layer thickness. This influence is particularly significant for the bending modes, and for the torsional modes to a limited extent. This is a significant result and needs further investigation in order to determine process parameters that can be used to produce a part with exact dynamic properties as that of a part made through other manufacturing processes.

Since natural frequency is directly proportional to stiffness and inversely proportional to mass, the slight decrease in the bending natural frequencies indicates a reduction in stiffness or an increase in mass. Since it is widely reported that the SLM process results in a slight reduction in density, the reduction in natural frequency can be completely attributed to a drop in bending

stiffness. However, the torsional modes demonstrate higher natural frequencies, regardless of process parameters. This could be attributed to the layer by layer build up used for the manufacturing process. The beams were excited and measured in a manner in which the direction of motion was perpendicular to the direction of the build layers. For torsion, this means that the planes between layers could have enhanced the stiffness of the part without exhibiting any significant influence on the bending modes. This result implies that the orientation of the build could play a major role in the stiffness properties and the natural frequencies of parts made by the SLM process. Having the layers running in one direction versus another could change the dynamic properties entirely.

5.2 Future Scope

As the SLM technology and additive manufacturing methods evolve, many aspects of properties of the parts need to be investigated further. The layer wise building method is seen to have a significant effect on the dynamic properties in general. Further studies need to be conducted in order to quantify the extent to which the build direction is responsible for changes in the dynamic response, and furthermore to determine the process parameters that may be used to overcome the influence of the build direction. This study was limited to a simple cantilever beam with a rectangular cross-section, it would be useful to conduct further tests with different geometries and different build directions. Rotating the part even a few degrees from vertical and changing the cross-section of each layer could have an impact on some of the properties. A study investigating this effect would be very useful in qualifying the process parameters. However, to fully comprehend the effects of the process parameters, it is important to conduct dynamic testing and fatigue testing on several end product with varying complex geometries.

Using complex parts and products for testing will give a better understanding of the process and its influence on a part that is used for specific applications. Complex geometries will also involve multiple angles, varying cross-sections, etc. that will change with every layer. This could further complicate the choice of process parameters, and therefore influence dynamic properties of the part. A simple part with constant cross-section could be rotated during the build set up to yield the required stiffness in various directions for its final application if a proper analysis is conducted on the part.

In addition to investigations into the build direction and geometry, it is important to conduct further testing of different DMLS materials. Materials such as aluminum, cobalt chrome, and titanium are alloys that are extensively used in manufacturing and studies must be conducted to see to what extent these findings hold true over different materials built using the same processes. This test was conducted using 316L stainless steel only in order to limit the scope of the study and fully understand the process parameters. Further tests must be conducted across each material offered by the manufacturer to determine the ability of the process to produce a part that has the required performance for the required application.

Build parameters have shown to have an influence on the properties of the final parts produced using DMLS. It is important to quantify the effect of these changes. A parameter such as layer thickness can have a major impact on the build. By increasing the layer thickness from 20 to 30 microns a substantial amount of the build time can be reduced. If a part can have similar properties as one made with the default parameter, but can be built faster by increasing the layer thickness, it would be a very useful option for manufacturers. However, it may not be viable due to some of the findings in this study. Further studies into the effects of layer thickness need to be conducted. These should be done in a manner in which the layer thickness is varied in smaller

increments, this can results in a better understanding of the layer thickness variable in conjunction with other process parameters.

REFERENCES

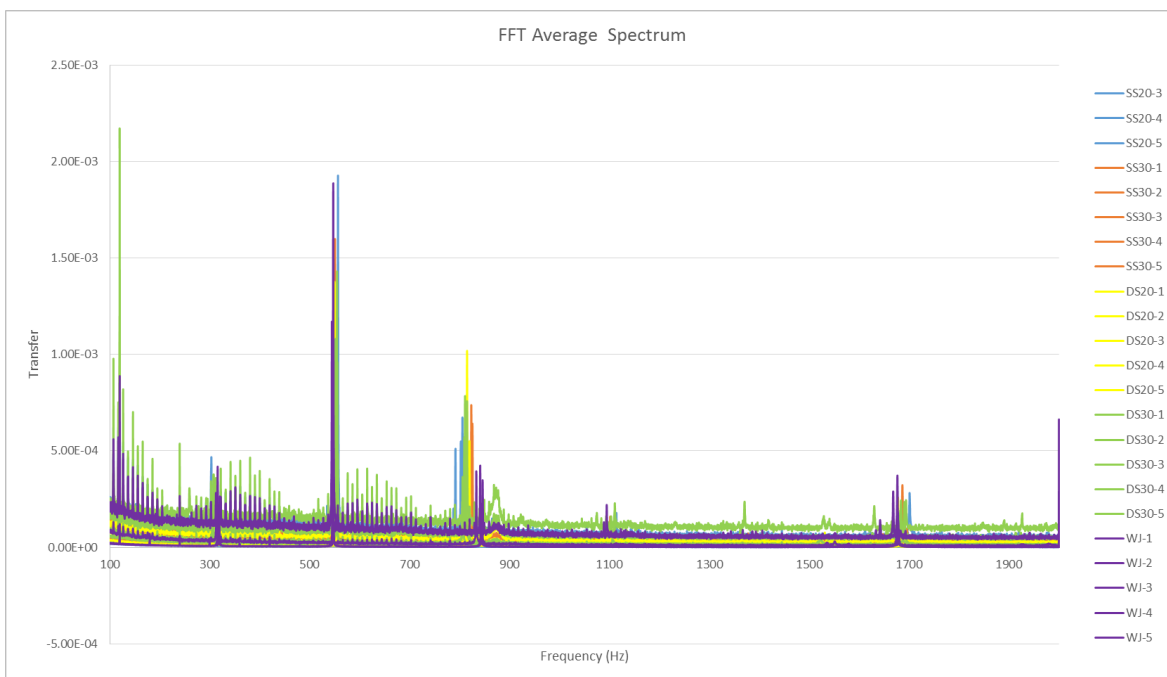
- Abe, F., Costa Santos, E., Kitamura, Y., Osakada, K., Shiomi, M. 2003. Influence of forming conditions on the titanium model in rapid prototyping with the selective laser melting process. *Proceedings of the Institution of Mechanical Engineers, Part C: Journal of Mechanical Engineering Science* 217 (1), pp. 119–126.
- ASTM E8/E8M-13a, 2013, “Standard Test Methods for Tension Testing of Metallic Materials,” ASTM International, West Conshohocken, PA
- ASTM Standard F2792 – 12a , 2015, "Standard Terminology for Additive Manufacturing Technologies," ASTM International, West Conshohocken, PA, 2015, www.astm.org.
- Casalino, G., Campanelli, S., Contuzzi, N., & Ludovico, A. (2014). Experimental investigation and statistical optimisation of the selective laser melting process of a maraging steel. *Optics & Laser Technology*, 65151-158. doi:10.1016/j.optlastec.2014.07.021
- Dai, D., & Gu, D. (2014). Thermal behavior and densification mechanism during selective laser melting of copper matrix composites: Simulation and experiments. *Materials And Design*, 55482-491. doi:10.1016/j.matdes.2013.10.006
- Damir, A. N. (2007). Prediction of fatigue life using modal analysis for grey and ductile cast iron. *International Journal of Fatigue*, 29(36), 499–507.
- David Bak, (2003) "Rapid prototyping or rapid production? 3D printing processes move industry towards the latter", *Assembly Automation*, Vol. 23 Iss: 4, pp.340 – 345
- EOS. (2014, January 1). History. Retrieved October 12, 2014, from http://www.eos.info/about_eos/history
- Hewitt, J. (2012, November 15). NASA 3D prints rocket parts — with steel, not plastic | ExtremeTech. Retrieved October 12, 2014, from <http://www.extremetech.com/extreme/140084-nasa-3d-prints-rocket-parts-with-steel-not-plastic>
- Jordan, C. (2014, May 14). RAPID.TECH 2014: EOS launches the EOS M 290 metal system to succeed the established EOSINT M 280 system. Retrieved October 5, 2014, from http://www.eos.info/eos_m_290_metal_additive_manufacturing_system
- J.P. Kruth, X. Wang, T. Laoui, L. Froyen, (2003) "Lasers and materials in selective laser sintering", *Assembly Automation*, Vol. 23 Iss: 4, pp.357 – 371
- Li, Y., & Gu, D. (2014). Thermal behavior during selective laser melting of commercially pure titanium powder: Numerical simulation and experimental study. *Additive Manufacturing*, 1-4(Inaugural Issue), 99-109. doi:10.1016/j.addma.2014.09.001
- Lou, A., & Grosvenor, C. (2012, December 7). Selective Laser Sintering, Birth of an Industry. Retrieved November 12, 2014, from http://www.me.utexas.edu/news/2012/0712_sls_history.php
- Ma, K. (2014, January 1). What's the Difference Between SLS and SLM - and Why Care? Retrieved October 6, 2014, from <http://www.rapidmade.com/rapidmade-blog/2014/6/30/ycjnxytvpt8n85gqtk5wj67cmx4t7>

- Noe. (2014, February 18). Production Methods: What's the Difference Between Selective Laser Sintering, Direct Metal Laser Sintering, Laser Melting and LaserCusing? Retrieved December 12, 2014, from http://www.core77.com/blog/materials/production_methods_whats_the_difference_between_selective_laser_sintering_direct_metal_laser_sintering_laser_melting_and_lasercusing_26457.asp
- Pacurar, R., Pacurar, A., Petrilak, A., & Balci, N. (2014). Finite Element Analysis to Predict the Mechanical Behavior of Lattice Structures Made by Selective Laser Melting Technology. *Applied Mechanics & Materials*, (657), 231. doi:10.4028/www.scientific.net/AMM.657.231
- Pr, N. (2014, May 6). Global 3D Printing (Polyjet, FDM, SLS, SLA) Market - Industry Analysis, Size, Share, Growth, Trends, and Forecast, 2013 - 2019. PR Newswire US.
- Quasicrystals Give 3DP Materials Greater Strength. (2014, November 5). Retrieved November 16, 2014, from <http://www.engineering.com/3DPrinting/3DPrintingArticles/ArticleID/8869/Quasicrystals-Give-3DP-Materials-Greater-Strength.aspx>
- Rao, S. s. (2011). *Mechanical Vibrations*. Upper Saddle River, NJ: Pearson Education
- Simonelli, M., Tse, Y., & Tuck, C. (2014). Effect of the build orientation on the mechanical properties and fracture modes of SLM Ti-6Al-4V. *Materials Science & Engineering: A*, 6161-11. doi:10.1016/j.msea.2014.07.086
- Swift, K. G. (2013). *Manufacturing Processes Selection Handbook*. Waltham, MA: Butterworth-Heinemann.
- Taek Bo, K., Sheng, Y., Ziyu, Z., Jones, E., Jones, J. R., & Lee, P. D. (2014). Additive manufactured porous titanium structures: Through-process quantification of pore and strut networks. *Journal Of Materials Processing Technology*, 214(11), 2706-2715. doi:10.1016/j.jmatprotec.2014.05.006
- Vorndran, E., Wunder, K., Moseke, C., Biermann, I., Müller, F., Zorn, K., & Gbureck, U. (2011). Hydraulic setting Mg₃(PO₄)₂ powders for 3D printing technology. *Advances in Applied Ceramics: Structural, Functional & Bioceramics*, 110(8), 476-481. doi:10.1179/1743676111Y.0000000030
- Vrancken, B., Cain, V., Knutsen, R., & Van Humbeeck, J. (2014). Residual stress via the contour method in compact tension specimens produced via selective laser melting. *Scripta Materialia*, 8729-32. doi:10.1016/j.scriptamat.2014.05.016
- Yasa, E. (2011). Microstructural investigation of Selective Laser Melting 316L stainless steel parts exposed to laser re-melting. *Procedia Engineering*, 19, 389-395.

APPENDIX A

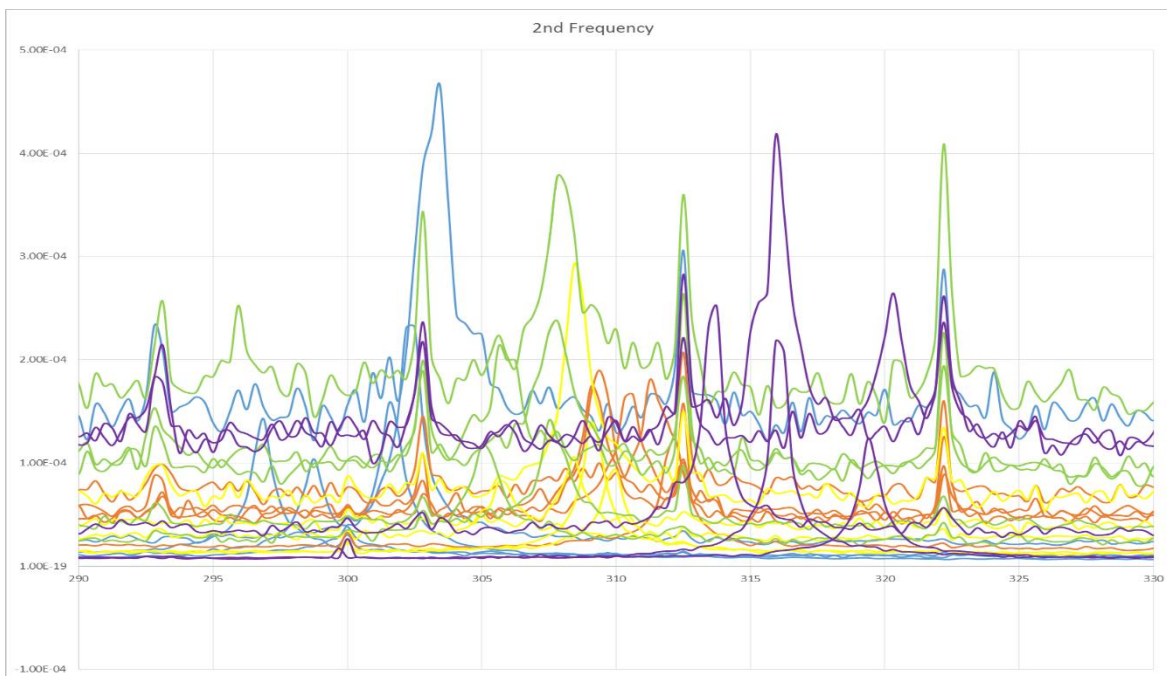
The following plots show the frequency response of all samples overlaid on each other.

Figure A 1



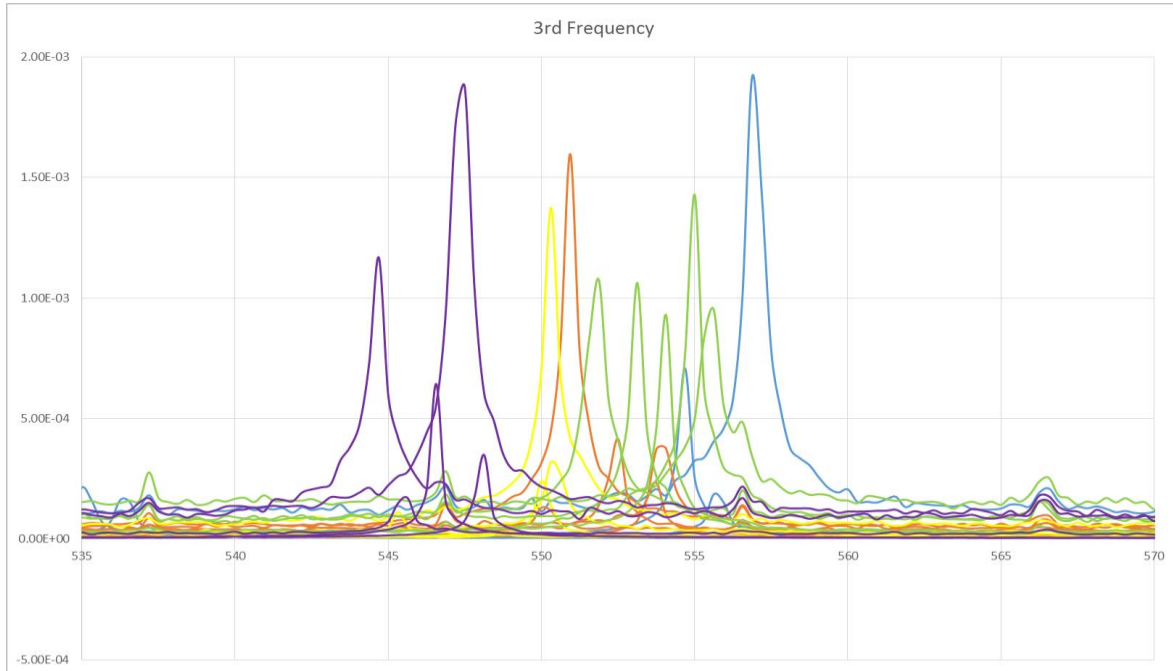
The following figure A2 shows the zoomed in 2nd frequency.

Figure A 2



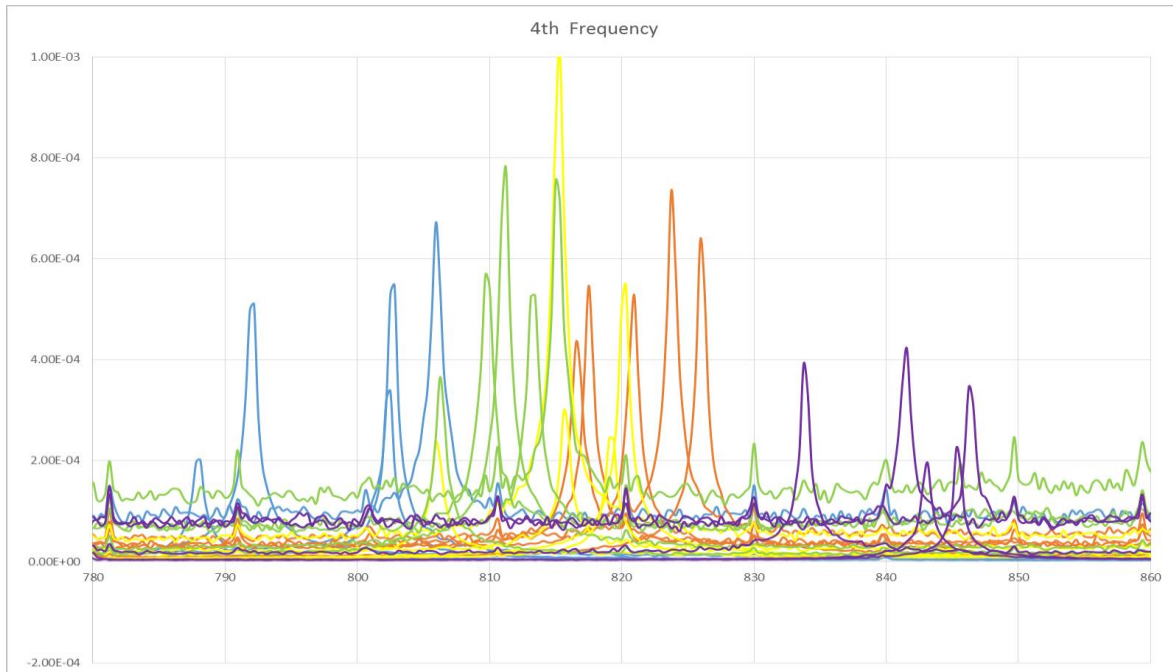
The following figure A3 shows the zoomed in 3rd frequency.

Figure A 3



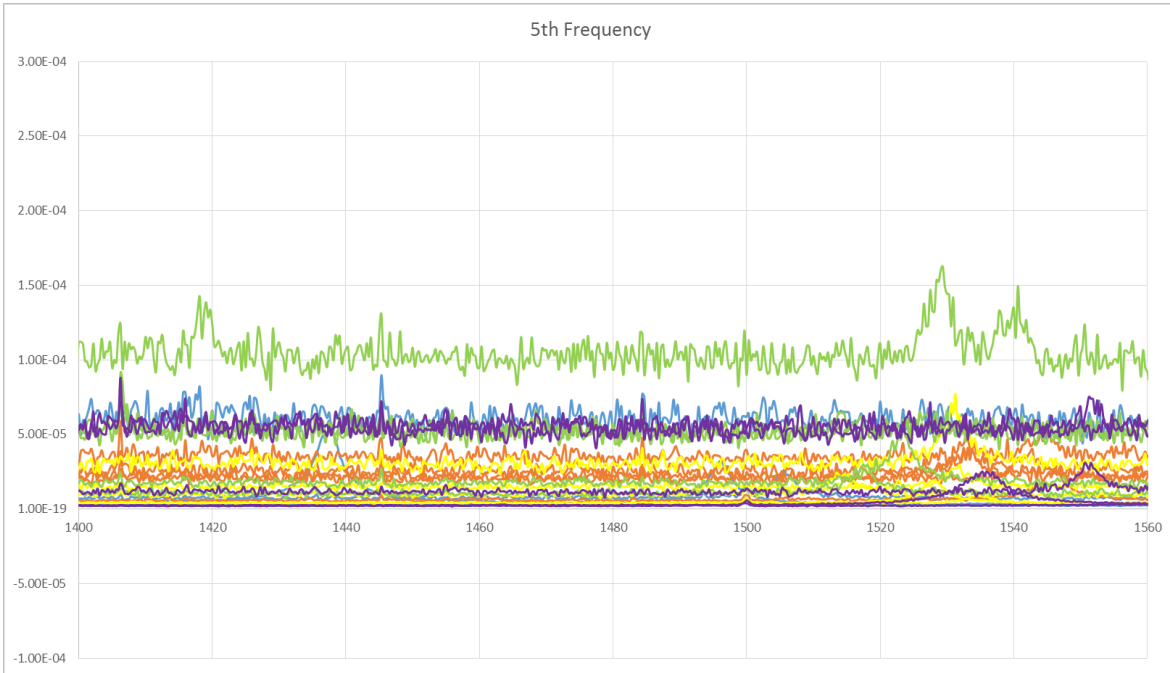
The following figure shows the zoomed in 4th frequency.

Figure A 4



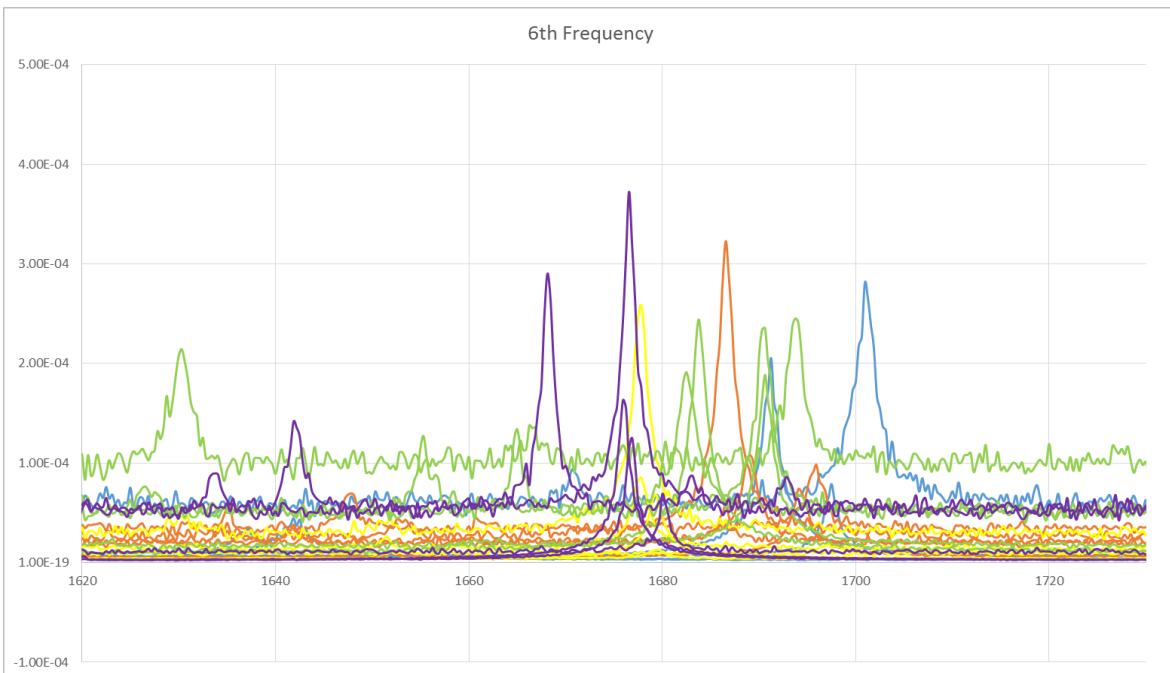
The following figure shows the zoomed in 5th frequency.

Figure A 5



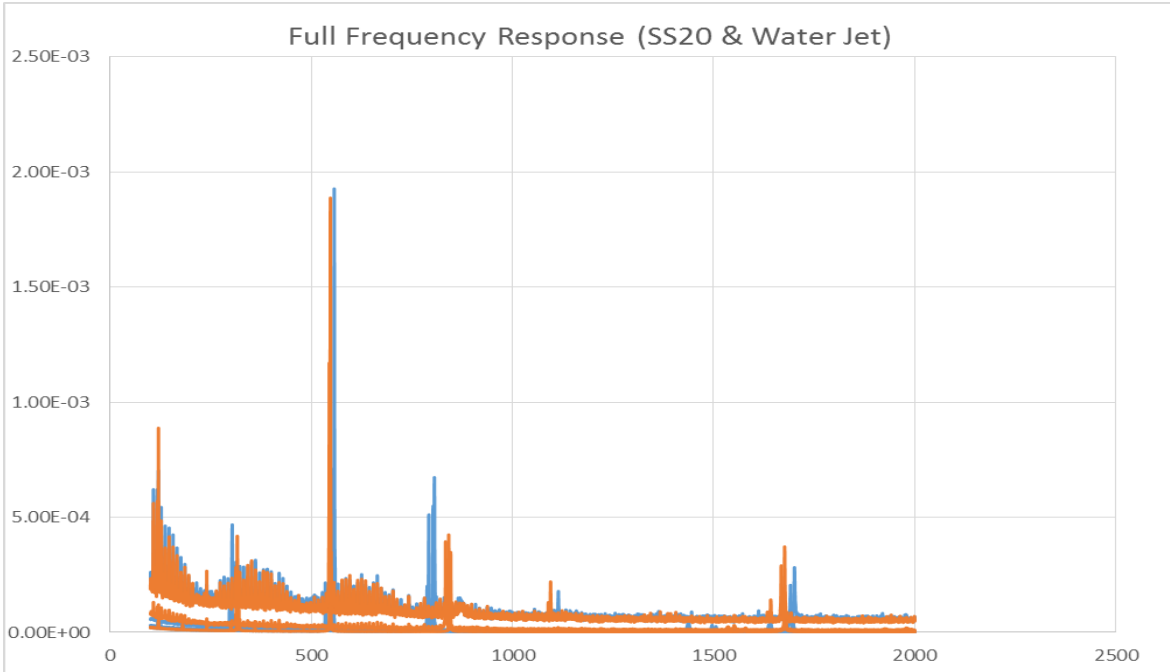
The following figure shows the zoomed in 6th frequency.

Figure A 6



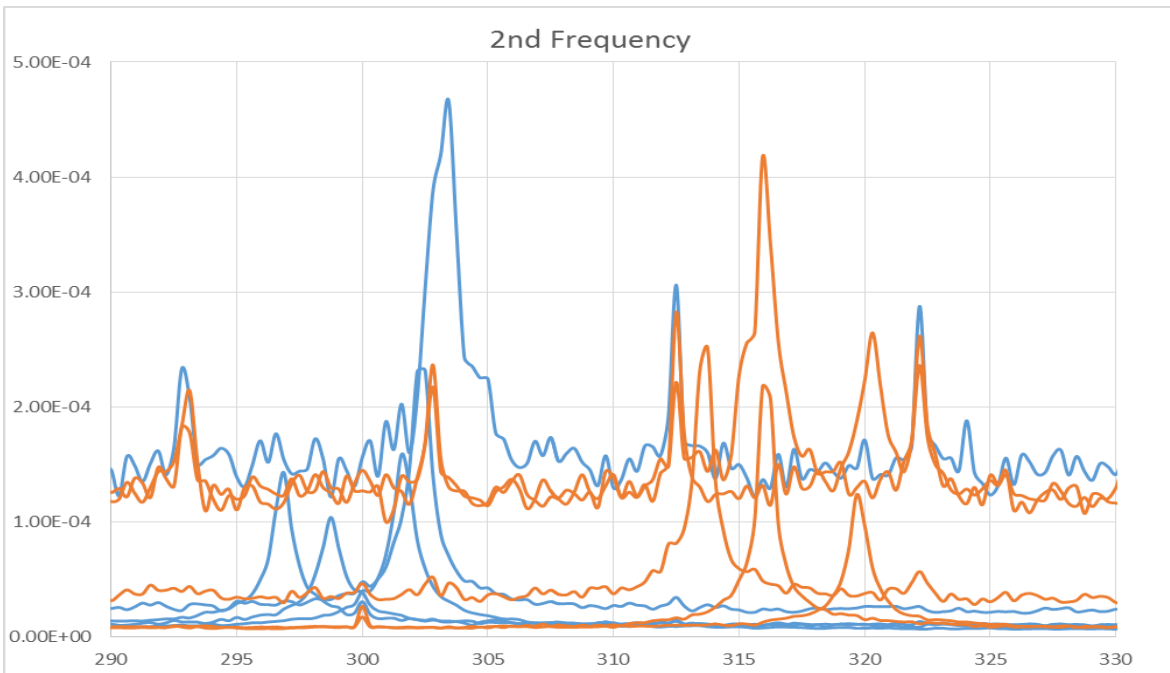
The full frequency response comparing the base build parameters (SS20) to the water jet cut material.

Figure A 7



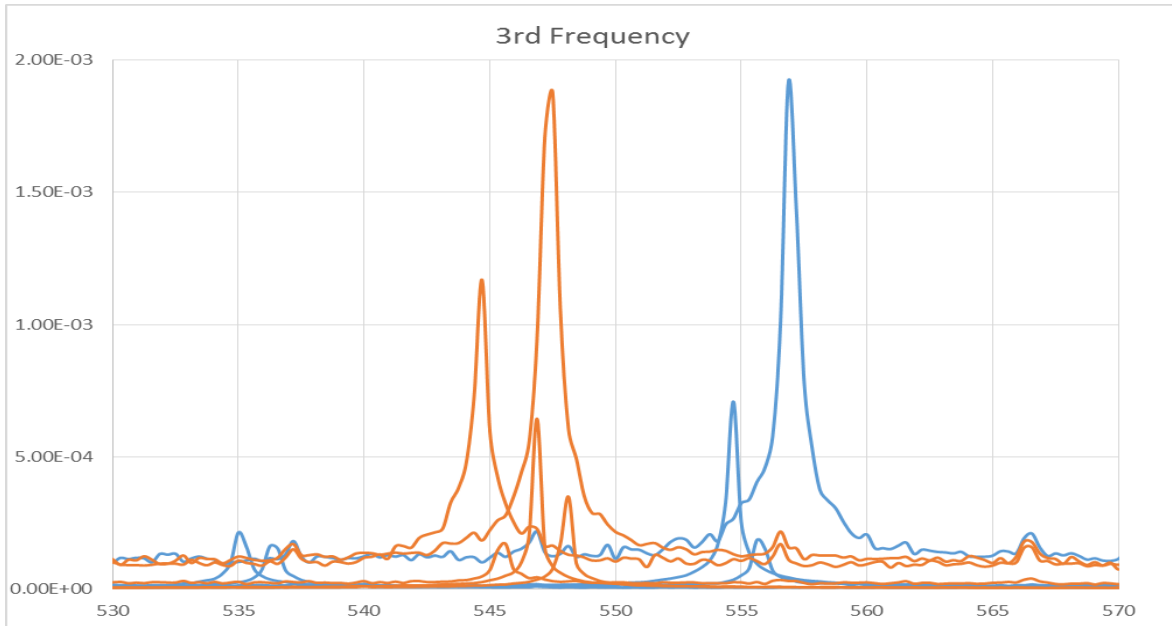
The following figure shows the zoomed in 2nd frequency comparing the base parameters to the water jet coupons.

Figure A 8



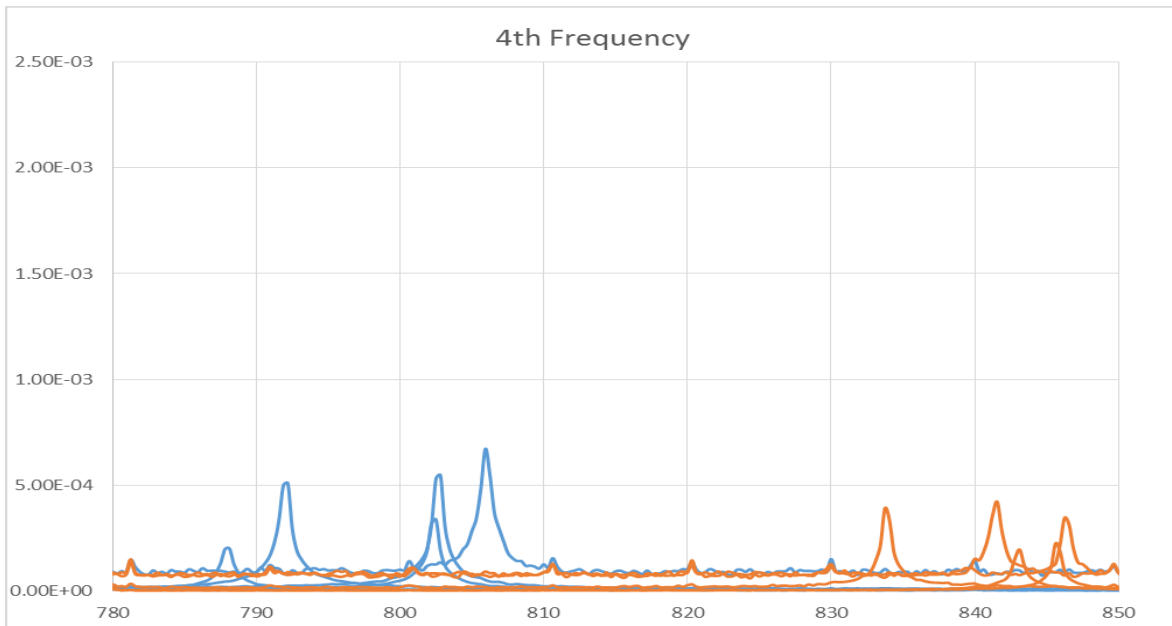
The following figure shows the zoomed in 3rd frequency comparing the base parameters to the water jet coupons.

Figure A 9



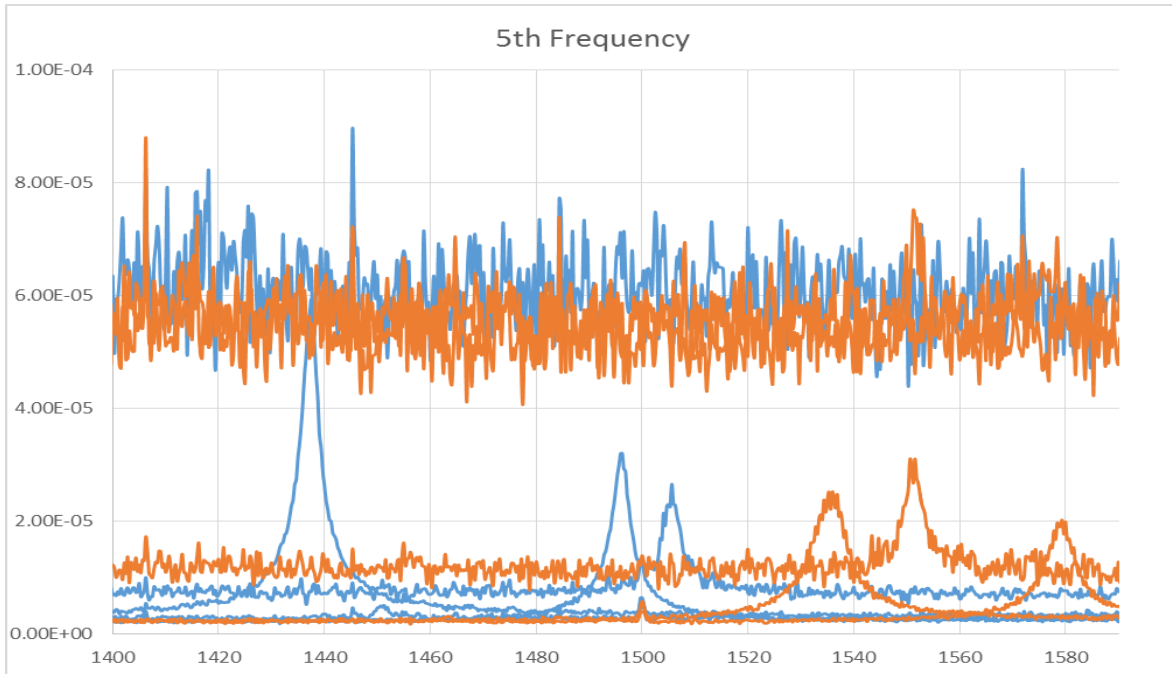
The following figure shows the zoomed in 4th frequency comparing the base parameters to the water jet coupons.

Figure A 10



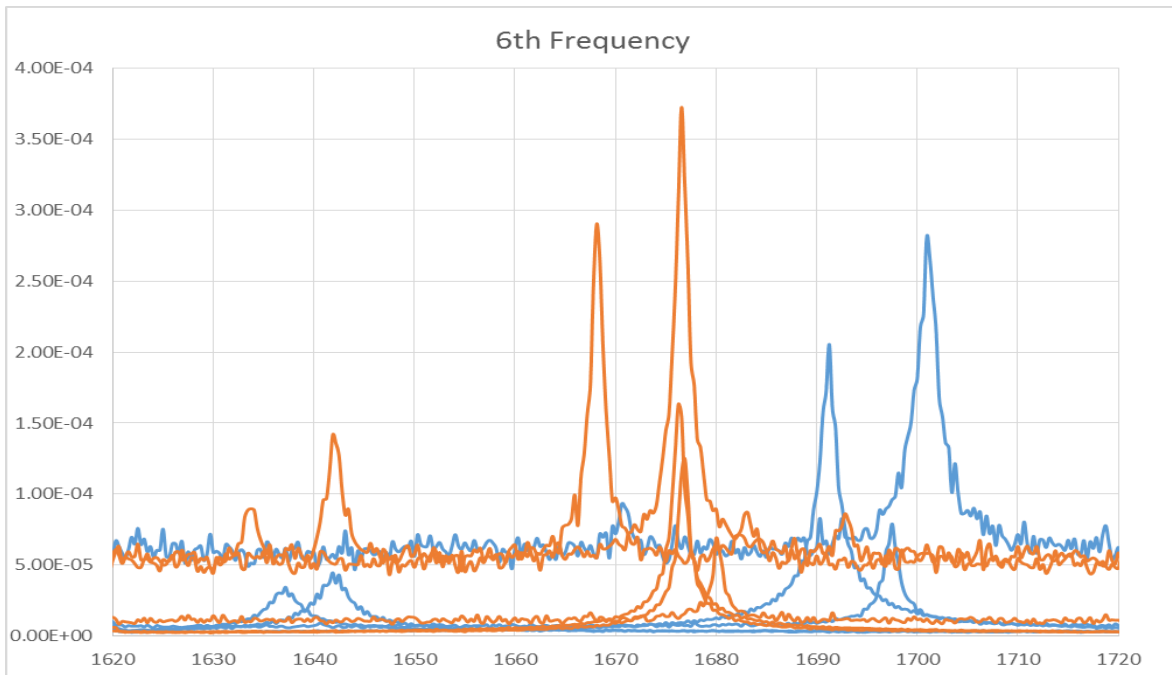
The following figure shows the zoomed in 5th frequency comparing the base parameters to the water jet coupons.

Figure A 11



The following figure shows the zoomed in 6th frequency comparing the base parameters to the water jet coupons.

Figure A 12



The Following table shows the hardness measurements taken for each sample along with the summary ANOVA table analyzing the data.

Table A 1

Harndess (HRA)						
	1	2	3	4	5	average
SS20	54.8	53	53	50.1	52.2	52.62
SS30	52.1	53.2	50.5	54.2	50.1	52.02
DS20	53.4	51.6	55.3	52.7	51.6	52.92
DS30	54.8	56.4	50.8	54.2	52.1	53.66
Water Jet	48.3	47.3	46.9	47	47.8	47.46
				Published hardness		49
Anova: Single Factor						
SUMMARY						
Groups	Count	Sum	Average	Variance		
SS20	5	263.1	52.62	2.892		
SS30	5	260.1	52.02	3.037		
DS20	5	264.6	52.92	2.357		
DS30	5	268.3	53.66	4.928		
Water Jet	5	237.3	47.46	0.343		
ANOVA						
Source of Variation	SS	df	MS	F	P-value	F crit
Between Groups	121.2496	4	30.3124	11.17961	6.28E-05	2.866081
Within Groups	54.228	20	2.7114			
Total	175.4776	24				

APPENDIX B

The following MatLab Code was used to simulate the bending beam and calculate the first three natural frequencies.

```
format compact
clear all
close all
clc

% Square Beam Deflection Equation

%dimension of beam (rectangular cross section)
%%
Width=.0381 ; %Width (m)
Height=.003175 ; %Height (m)
Length=.2159 ; %Length of Beam (m)
density=7990.0 ; %Material Density 316L (in kg/m^3)
mb=density*Length*Width*Height ; %Mass of the beam
Mass=(.23)*(mb) ; % Equivilent mass at end of beam (kg)
Mass1=(mb) ; %total mass of beam

%Constants
E=193000000000 ; %Modulus of Elasticity 316L steel (Pa)
Force=-10 ; %Static Load (N)
% X=.5 ; %Point of deflection/stress meaurment for static load

%Moment of Inertia
I=(Width*Height^3)/12 ;

%Section Modulus
Z=(Width*Height^2)/6;

%Stiffness equivilent
K=(3*E*I)/(Length^3);

%number of points tested
N=.0001; %increment value
points=[0:N:Length];

%time of test (s)
t=50;
Time=0:.1:t;

% % USE THIS PART TO SIMULATE STATIC LOAD (UN% W also)
%array to extract data from loop
def=[];
for X = 0:N:Length

    Deflection=((Force*X^2)/(6*E*I))*(3*Length-X);

    def=[def,Deflection];
```

```

end

figure(1)
plot(points,def)
title('bending beam')
grid on
xlabel('length (m)')
ylabel('Deflection (m)')
%
% for T = Time
%
%   F = -50*sind(100*T);

% %array to extract data from loop
% def=[];
%
% for X = 0:.01:L
%
%   Deflection=((F*X^2)/(6*E*I))*(3*L-X);
%
%   def=[def,Deflection];
%
% end
%
% hold on
% figure(1)
% plot(points,def)
% title('bending beam')
% xlabel('Beam Length (cm)')
% ylabel('Deflection (m)')
%
% end

%Frequency response SIMPLIFIED Equivalent Mass
zeta=.02;
C=zeta*sqrt(2*Mass*K);
transfer=[];
W=0:0.1:1200;
for w = W

    Trans=(1/((-Mass*w^2)+(j*C*w)+K)) ;

    transfer=[transfer,Trans] ;

end
freq1=(((1.875014)^2)*sqrt((E*I)/(Mass1*Length^3)))/(2*pi)
freq2=(((4.694091)^2)*sqrt((E*I)/(Mass1*Length^3)))/(2*pi)
freq3=(((7.854757)^2)*sqrt((E*I)/(Mass1*Length^3)))/(2*pi)

hold on
figure(2)
plot(W/(2*pi),20*log10(abs(transfer)))

```

```

title('Frequency Response')
xlabel('Frequency hz')
ylabel('Transfer Function')
grid on

% Cantilever MODE SHAPES
beta1=(1.875104/Length);
beta2=(4.694091/Length);
beta3=(7.854757/Length);
alpha1=((sin(beta1*Length)+sinh(beta1*Length))/(cos(beta1*Length)+cosh(beta1*Length)));
alpha2=((sin(beta2*Length)+sinh(beta2*Length))/(cos(beta2*Length)+cosh(beta2*Length)));
alpha3=((sin(beta3*Length)+sinh(beta3*Length))/(cos(beta3*Length)+cosh(beta3*Length)));

mode1=[];
mode2=[];
mode3=[];
for x=0:N:Length

    y1=(sin(beta1*x)-sinh(beta1*x)-alpha1*(cos(beta1*x)-cosh(beta1*x)));
    y2=(sin(beta2*x)-sinh(beta2*x)-alpha2*(cos(beta2*x)-cosh(beta2*x)));
    y3=(sin(beta3*x)-sinh(beta3*x)-alpha3*(cos(beta3*x)-cosh(beta3*x)));

    mode1=[mode1,y1];
    mode2=[mode2,y2];
    mode3=[mode3,y3];

end

figure(3)
plot(points,mode1/5)
title('Mode 1 First Bending')
grid on

figure(4)
plot(points,mode2/60)
title('Mode 2 Second Bending')
grid on

figure(5)
plot(points,mode3/1400)
title('Mode 3 Third Bending')
grid on

% %FULL FREQ RESPONSE Simply Supported
% TL=Length ; % test location
% freqresponse=[];
% for w = W
%
%   FreqR = (2/mb)*(((1/((freq1^2)-(w^2)))*(sin(1*pi)*sin((1*pi*TL)/Length)))+(1/((freq2^2)-
(w^2)))*(sin(2*pi)*sin((2*pi*TL)/Length)))+(1/((freq3^2)-(w^2)))*(sin(3*pi)*sin((3*pi*TL)/Length)));
%
%   freqresponse = [freqresponse,FreqR];
% end

```

```

%
% figure(6)
% plot(W,abs(freqresponse))
% line([freq1,freq1],ylim)
% line([freq2,freq2],ylim)
% line([freq3,freq3],ylim)

%Full Cantilever Frequency response
TL=Length ; %test location
X1=(sin(beta1*Length)-sinh(beta1*Length))-alpha1*(cos(beta1*Length)-cosh(beta1*Length));
X2=(sin(beta2*Length)-sinh(beta2*Length))-alpha2*(cos(beta2*Length)-cosh(beta2*Length));
X3=(sin(beta3*Length)-sinh(beta3*Length))-alpha3*(cos(beta3*Length)-cosh(beta3*Length));
Xs1=(sin(beta1*TL)-sinh(beta1*TL))-alpha1*(cos(beta1*TL)-cosh(beta1*TL));
Xs2=(sin(beta2*TL)-sinh(beta2*TL))-alpha2*(cos(beta2*TL)-cosh(beta2*TL));
Xs3=(sin(beta3*TL)-sinh(beta3*TL))-alpha3*(cos(beta3*TL)-cosh(beta3*TL));

FFT=[];
for w = W
    H1=1/((freq1^2)-(w^2)+2*j*w*freq1*zeta);
    H2=1/((freq2^2)-(w^2)+2*j*w*freq2*zeta);
    H3=1/((freq3^2)-(w^2)+2*j*w*freq3*zeta);

    freq_response = (1/(density*(Height*Width)))*((X1*(Xs1)*H1*w)+(X2*(Xs2)*H2*w)+(X3*(Xs3)*H3*w));
    FFT=[FFT,freq_response];
end

figure(7)
plot(W,abs(FFT))
line([freq1,freq1],ylim)
line([freq2,freq2],ylim)
line([freq3,freq3],ylim)
xlabel('Frequency (hz)')
ylabel('Transfer Function')
title('Full Frequency Response')

```

The following MatLab script was used to post process the vibrometer data to extract the peak values and calculate the damping ratios for each.

```
clear all
close all
format compact
clc

% IMPORT DATA
%INPUT DATA FILE NAME

DATA=xlsread('SS20_5');

%Seperate into FREQ AND VELOC

FREQ=DATA(:,1);
VELOC=DATA(:,2);

%PLOT DATA

plot(FREQ,VELOC),grid
xlabel('Frequency (Hz)'),ylabel('Velocity (mm/s)')

%SET FREQUENCY RANGES
% w1=;
W2=300:.3125:305;
W3=553:.3125:557;
W4=795:.3125:806;
W5=1501:.3125:1507;
W6=1693:.3125:1701;

% i1=find(FREQ>=min(W1) & FREQ<=max(W1));
i2=find(FREQ>=min(W2) & FREQ<=max(W2));
i3=find(FREQ>=min(W3) & FREQ<=max(W3));
i4=find(FREQ>=min(W4) & FREQ<=max(W4));
i5=find(FREQ>=min(W5) & FREQ<=max(W5));
i6=find(FREQ>=min(W6) & FREQ<=max(W6));

% VELOC1=VELOC(i1);
VELOC2=VELOC(i2);
VELOC3=VELOC(i3);
VELOC4=VELOC(i4);
VELOC5=VELOC(i5);
VELOC6=VELOC(i6);

% FREQ1=W1;
FREQ2=W2;
FREQ3=W3;
FREQ4=W4;
FREQ5=W5;
FREQ6=W6;
```

```

%Extract wn2
[Y2,I2]=max(VELOC2);
wn2=FREQ2(I2)% this is the calculated natural frequency
hpp2=Y2/sqrt(2);

b2=find(hpp2-0.1<=VELOC2 & VELOC2<=hpp2+0.1);
w21=FREQ2(b2(1));
w22=FREQ2(b2(2));
zeta2=(w22-w21)/wn2% this is the calculated damping ratio

%Extract wn3
[Y3,I3]=max(VELOC3);
wn3=FREQ3(I3)% this is the calculated natural frequency
hpp3=Y3/sqrt(2);

b3=find(hpp3-0.1<=VELOC3 & VELOC3<=hpp3+0.1);
w31=FREQ3(b3(1));
w32=FREQ3(b3(2));
zeta3=(w32-w31)/wn3% this is the calculated damping ratio

%Extract wn4
[Y4,I4]=max(VELOC4);
wn4=FREQ4(I4)% this is the calculated natural frequency
hpp4=Y4/sqrt(2);

b4=find(hpp4-0.1<=VELOC4 & VELOC4<=hpp4+0.1);
w41=FREQ4(b4(1));
w42=FREQ4(b4(2));
zeta4=(w42-w41)/wn4% this is the calculated damping ratio

%Extract wn5
[Y5,I5]=max(VELOC5);
wn5=FREQ5(I5)% this is the calculated natural frequency
hpp5=Y5/sqrt(2);

b5=find(hpp5-0.1<=VELOC5 & VELOC5<=hpp5+0.1);
w51=FREQ5(b5(1));
w52=FREQ5(b5(2));
zeta5=(w52-w51)/wn5% this is the calculated damping ratio

%Extract wn6
[Y6,I6]=max(VELOC6);
wn6=FREQ6(I6)% this is the calculated natural frequency
hpp6=Y6/sqrt(2);

b6=find(hpp6-0.1<=VELOC6 & VELOC6<=hpp6+0.1);
w61=FREQ6(b6(1));
w62=FREQ6(b6(2));
zeta6=(w62-w61)/wn6% this is the calculated damping ratio

```